

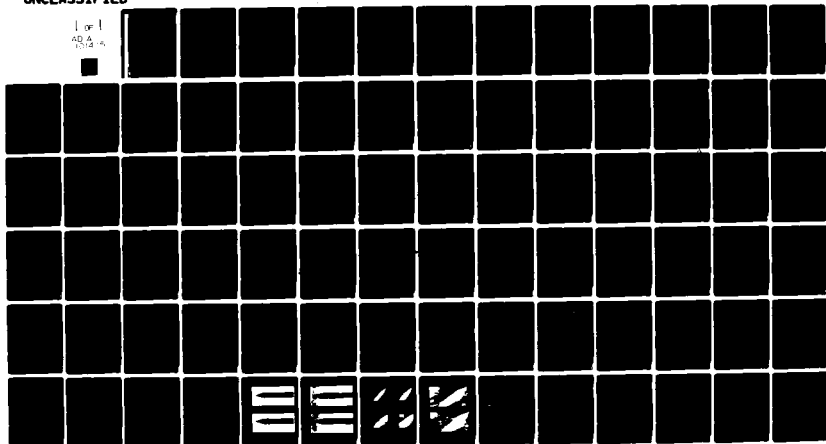
AD-A101 415

TECHNION - ISRAEL INST OF TECH HAIFA DEPT OF AERONAU-ETC F/G 20/4
INVESTIGATION OF NON LINEAR AERODYNAMIC CHARACTERISTICS OF SLEM-ETC(U)
DEC 80 J ROM, D ALMOSINO DA-ERO-78-6-119

NL

UNCLASSIFIED

1 of 1
40 A
11-12-80



END
DATE
FILED
8-81
DTIC

FILE COPY

DA 101415

TC

(12)

LEVEL

AD

INVESTIGATION OF NON LINEAR AERODYNAMIC CHARACTERISTICS
OF SLENDER BODIES AT HIGH INCIDENCE, IN
SUBSONIC AND TRANSONIC SPEEDS.

FINAL TECHNICAL REPORT

by

J. ROM and D. ALMOSNINO

DECEMBER 1980.

EUROPEAN RESEARCH OFFICE
UNITED STATES ARMY
LONDON, ENGLAND

DTIC
ELECTED
JUL 15 1981
S D

A

GRANT NO. DAERO-78-G-119

DEPARTMENT OF AERONAUTICAL ENGINEERING
TECHNION - ISRAEL INSTITUTE OF TECHNOLOGY
HAIFA, ISRAEL.

APPROVED FOR PUBLIC RELEASE: DISTRIBUTION UNLIMITED.

81 7 14 005

AD

6
INVESTIGATION OF NON LINEAR AERODYNAMIC CHARACTERISTICS
OF SLENDER BODIES AT HIGH INCIDENCE, IN
SUBSONIC AND TRANSONIC SPEEDS.

11
FINAL TECHNICAL REPORT.

by

11 J. ROM D. ALMOSNINO

11 DECEMBER 1980 /

12) 21

EUROPEAN RESEARCH OFFICE

UNITED STATES ARMY

LONDON, ENGLAND

15/12
GRANT NO. DAERO-78-G-119

DEPARTMENT OF AERONAUTICAL ENGINEERING
TECHNION - ISRAEL INSTITUTE OF TECHNOLOGY
HAIFA, ISRAEL.

APPROVED FOR PUBLIC RELEASE: DISTRIBUTION UNLIMITED.

11/11

ABSTRACT

This report presents the results of the experimental investigation of the effect of small, symmetric jet injection from the nose of a slender body on the lateral forces and moments at high incidence. The investigation includes the effects of Mach and Reynolds numbers rate of injection and the position of injection. It is demonstrated that at low speeds of jet blowing even small rates are a very useful means of side-force and yawing moment alleviation and even control, influencing both separation and structure of the vortex field. Such effects are also obtained at high subsonic and even transonic Mach numbers but require much higher injection rates. The results of some visualization tests are also included for better understanding and interpretation of the flow phenomena involved. The report includes also presentation of some preliminary results of a method for the calculation of the longitudinal aerodynamic characteristics of bodies at incidence including the separation of symmetric vortices, in subsonic flow. Preliminary results of the prediction method which consists of a combined source/vortex lattice model, are presented. This method is being further developed for calculations of the aerodynamic characteristics of more complex wing-body configurations of high angles of attack.

TABLE OF CONTENTS

	<u>PAGE No.</u>
ABSTRACT	I
TABLE OF CONTENTS	II - III
LIST OF SYMBOLS	IV - V
LIST OF FIGURES	VI - VII
1. INTRODUCTION	1 - 2
2. THE EFFECTS OF SYMMETRIC JET INJECTION FROM THE NOSE OF A SLENDER BODY ON THE LATERAL FORCES AND MOMENTS AT HIGH INCIDENCE	3 - 18
2.1. Lateral Behaviour of Slender Bodies at High Angles of Attack, at Subsonic and Transonic Speeds.	3 - 6
2.2. Methods for the Suppression and Control of the Side Force and Yawing Moment at High Incidence in Zero Side-Slip	6 - 7
2.3. Studies of Side Force and Yawing Moment Alleviation and Control on a Cone-Cylinder Body at High Angles of Attack, using Small Symmetrical Jets Injected from the Nose at Subsonic and Transonic Mach Numbers.	7 - 18
2.3.1. The Model and the Experimental Facilities	7 - 9
2.3.2. Results	9 - 18
3. A METHOD FOR THE CALCULATION OF THE LONGITUDINAL AERO- DYNAMIC CHARACTERISTICS OF BODIES AT ANGLES OF ATTACK, INCLUDING SYMMETRIC VORTEX SEPARATION IN SUBSONIC FLOW	19 - 28
3.1. State of the Art	19 - 20
3.2. The Proposed Computational Method for Incompressible Flow	20 - 25
3.3. Results of Calculations	25 - 28
3.3.1. Computational Aspects and Problems	25 - 28
3.3.2. Preliminary Results Compared to Experimental Data and to other Analytical Methods	28
4. CONCLUSIONS	29 - 30
4.1. The Effects of Jet Injection on the Lateral Forces and Moments at High Angles of Attack in Subsonic and Trans- sonic Flow.	

TABLE OF CONTENTS
(CONTINUED)

	<u>PAGE No.</u>
4.2. Calculations of the Flow over Bodies at Incidence in Subsonic Flow, Including the Effects of Symmetric Vortex Separa- tion.	29 - 30
REFERENCES	31 - 37
FIGURES	38 - 73

LIST OF SYMBOLS

C_{D_i}	induced drag coefficient $D/qS_{ref.}$
C_L	lift coefficient L/qS_{ref}
C_n	yawing moment coefficient, N/qS_{ref}^d
C_M	pitching moment coefficient, M/qS_{ref}^d
C_{NOR}	normal force coefficient, $F_{NOR}/qS_{ref.}$
C_p	pressure coefficient $\frac{p - p_\infty}{q}$
C_Y	side force coefficient, $Y/qS_{ref.}$
C_u	blowing rate coefficient. $\dot{m}_j u_j/qS_{ref.}$
$d, C_{ref.}$	reference chord (body diameter)
D	induced drag force
F_{NOR}	normal force to the body
H	geometrical influence coefficients matrix
i	index
j	index (or subscript for "jet")
K	strength of vortex segment
L	lift force
\dot{m}_j	jet mass flow rate
M	Mach number
M, N	pitching and yawing moments (about nose tip point)
n_x, n_y, n_z	direction cosines of the vector normal to an elemental panel
N_c	number of sub-divisions, axial direction

- V -

N_s	number of sub-divisions, circumferential direction
P	static pressure
P_∞	static pressure of the free stream
q	dynamic pressure, $\frac{1}{2} \rho V^2$
Re_d	Reynolds number, based on body diameter, $\frac{\rho V d}{\mu}$
S	strength of source/sink
S_{ref}	reference area (body cross section, $\frac{\pi d^2}{4}$)
ΔS	area of an elemental panel
U, V	free stream velocity
u, v, w	velocity disturbance in (x, y, z) directions, accordingly
u_j	theoretical velocity (assuming fully expanded isentropic flow)
v_n	normal component of free stream velocity
x, y, z	Cartezian coordinates of a point
$\Delta x, \Delta y, \Delta z$	components of a segment, in (x, y, z) directions, accordingly
x_{CP}	center of pressure position
Y	side force
α	angle of attack
ρ	air density
ϕ, θ	geometrical angles
μ	air viscosity

NOTE: All forces and moments are given in body axes of reference, for the experimental results.

SPECIAL SUBSCRIPTS

o	denotes at $\alpha = 0$
a	denotes at $\alpha \neq 0$
ref	reference

LIST OF FIGURES

FIGURE No.

1. The cone-cylinder model.
2. Normal force and pitching moment coefficients vs. angle of attack, $V = 32$ m/sec, no injection.
3. Side force coefficient vs. angle of attack, $V = 32$ m/sec, no injection.
4. Yawing moment coefficient vs. angle of attack, $V = 32$ m/sec, no injection.
5. Variation of side force coefficient vs. blowing rate coefficient, at various angles of attack, $V = 32$ m/sec, no transition strip.
6. Variation of yawing moment coefficient vs. blowing rate coefficient, at various angles of attack, $V = 32$ m/sec, no transition strip.
7. Variation of side force coefficient vs. blowing rate coefficient, at various angles of attack, $V = 32$ m/sec, with transition strip at $x/d = 0.333$.
8. Variation of yawing moment coefficient vs. blowing rate coefficient, at various angles of attack, $V = 32$ m/sec, with transition strip at $x/d = 0.333$.
9. Normal force coefficient and pitching moment coefficient vs. blowing rate coefficient, at various angles of attack, $V = 32$ m/sec, no transition strip.
10. Normal force coefficient and pitching moment coefficient vs. blowing rate coefficient, at various angles of attack, $V = 32$ m/sec, with transition strip at $x/d = 0.333$.
11. Blowing rate coefficient needed for side force alleviation at various angles of attack.
12. Variation of side force coefficient vs. angle of attack for different amounts of blowing rate coefficient, for windward and leeward jet blowing.
13. Amount of blowing rate coefficient needed for side force alleviation at various angles of attack.
14. Amount of blowing rate coefficient needed for side force alleviation for various amounts of sideforce.

LIST OF FIGURES (CONT'D)

15. Normal forces and pitching moment coefficient vs. Mach number, at two angles of attack, no transition strip, no injection.
16. Side force and yawing moment coefficient vs. Mach number, at two angles of attack, to transition strip, no injection.
17. Side force coefficient vs. angle of attack at various Mach numbers, no injection, no transition strip.
18. Yawing moment coefficient vs. angle of attack at various Mach numbers, no injection, no transition strip.
19. Side force and yawing moment coefficients vs. blowing rate coefficient at $M = 0.4$, at two angles of attack, no transition strip.
20. Side force and yawing moment coefficients vs. blowing rate coefficient at $M = 0.7$, at two angles of attack.
21. Side force and yawing moment coefficients vs. blowing rate coefficient at $M = 0.85$, at 47° angle of attack.
22. Normal force and side force coefficients vs. Reynolds number, at various angles of attack, no transition strip, no injection.
23. Pitching moment coefficient, vs. Reynolds number at various angles of attack, no transition strip.
24. Yawing moment coefficient vs. Reynolds number, at various angles of attack, no transition strip.
25. Oil flow visualization of the cone-cylinder model at $V = 32$ m/sec, $\alpha = 40^\circ$, with a transition ring at $x/D = 0.333$.
26. Oil flow visualization of the cone-cylinder model at $V = 32$ m/sec, $\alpha = 55^\circ$, no transition ring.
27. Schlieren photographs of the cone-cylinder model at various Mach numbers, $\alpha = 47^\circ$, no jet blowing.
28. Schlieren photographs of the cone cylinder model at $M = 0.7$, $\alpha = 37.5^\circ$ with and without jet blowing.
29. Illustration of the model for bodies including vortex separation.
30. Schematic flow-chart of the method of calculation.
31. Pressure distribution on a sharp cone-cylinder body at $\alpha = 0^\circ$.

1. INTRODUCTION

This report summarizes the research performed under Grant No. DAERO-78-G-119 during the period September 1st 1978 to September 30th, 1980.

Many modern aircraft and missiles are being designed for high angle of attack performance, in order to get improved maneuverability and flight envelope at subsonic and transonic speeds. However the flow phenomena involved in high angle of attack flight are rather complicated. Some of these complex flow phenomena are related to the slender wing-body configuration which is typical to the modern missiles and combat aircraft. The vortex system which the slender body sheds at high incidence causes a non-linear behavior of the aerodynamic coefficients, and it causes also considerable interaction with wing and tail surfaces. Furthermore, at higher incidence an asymmetric vortex flow pattern is established causing considerable side forces and yawing moments even at zero sideslip. At such high incidence there are also strong viscous effects (such as vortex breakdown), which complicate even further the description of the flow phenomena.

This report summarizes the results of 3 years of research during which efforts were concentrated on two main aspects of the aerodynamics of bodies at high angles of attack.

- (1) An experimental investigation of the effect of small symmetric jet injection from the nose of a slender body on the lateral forces and moments at high incidence.

The purpose of this investigation is to develop an active control system by means of which alleviation and even manipulation of side forces and yawing

moments can be achieved at high angles of attack at zero sideslip. The investigation includes the influence of the following parameters. Mach and Reynolds Numbers, transition strips, rate of injection, and the position of the injecting stations. Visualization tests were also performed, for better understanding and interpretation of the results. The development of this experimental work was reported in previous publications [1,2,3,4].

- (2) Development of a method for the calculation of the longitudinal characteristics of bodies at angle of attack, including symmetric vortex separations, in subsonic flow. Preliminary results of a combined source/vortex lattice method, are presented in this report. This computational method seems encouraging enough for further development, and can be expected to enable detailed calculation of complex wing-body configurations in the future.

2. THE EFFECTS OF SYMMETRIC JET INJECTION FROM THE NOSE OF A SLENDER BODY ON THE LATERAL FORCES AND MOMENTS AT HIGH INCIDENCE.

2.1. Lateral Behaviour of Slender Bodies at High Angles of Attack, at Subsonic and Transonic Speeds.

Separation of the boundary layer occurs at moderate angle of attack because of the adverse cross flow pressure gradient on the leeward side of the slender body. The separated boundary layer then rolls-up to form a system of distinct vortices. (The description of separation is more complicated when the body is not slender [5,6]).

The rolled up vortex sheet may stay close to the body and be continuously fed from the separated boundary layer, or it may leave the body entirely further downstream. Separation line may be expected to be found near the line of minimum pressure coefficient on the leeward side of the body, since the separation is caused by the adverse pressure gradient [7,].

Due to geometrical irregularities of the nose of the body and irregularities in the outer flow, one side of the boundary layer may separate first from the body, maintaining a certain vortex strength in the corresponding rolled-up vortex sheet. The other side of the boundary layer may remain attached and separate only further downstream on the body with a corresponding stronger vortex. In this manner the asymmetric vortex system is generated behind the body at high angles of attack. This description is supported for example by results presented in Ref. 8 where it is shown that the side forces are associated with the asymmetry of circumferential pressure distribution and the asymmetry of the vortex sheet separation. The separation line is shifted towards the windward side of the body as the

angle of incidence is increased [7]. Measurement of the circumferential angles of separation indicate that asymmetry of the separation increases as the angle of incidence is increased (in laminar boundary layer conditions). The maximum angular difference nearly coincided with the maximum measured side force. (Maximum angular difference was of the order of 20° to 40° for sharp slender nose shapes). It was found that as the angle of attack was high enough, several vortex separations occurred along the body [7, 8,9].

As it seems from the state of the art today, it is generally accepted that the following phenomenological rules associated with flow asymmetry hold true:

- (1) Initial direction of the side force and yawing moment is unpredictable because of its connection with small irregularities in nose geometry. However, once the direction is established, it does not change for given geometry and flow conditions.
- (2) Magnitude of the side force increases with the increasing finesse ratio of the nose.

The nose shape is a most significant parameter which affects the side forces [10, 11, 12, 13]. Blunt nose tips reduce the magnitude of the side force and yawing moment. Refs. [14,15,16, 17,18], for example show that the roll angle of the nose about the body axis of revolution has a most considerable effect on the sign and magnitude of side force and yawing moment.

(3) The magnitude of the side force depends on the angle of incidence. Change of sign may occur as the angle of incidence is increased, (even more than once).

Side forces and yawing moments are very small below $\alpha = 25^\circ$. Beyond this they increase quite sharply and reach their peaks between $35^\circ - 50^\circ$, depending on the Reynolds and Mach numbers and on the geometry of the configuration.

(4) Reynolds number has almost no effect on the angle of incidence for the onset of the asymmetry, but it has a notable effect on the magnitude of the side force.

Some information about the effects of Reynolds number and of Mach number on lateral forces and moments at zero sideslip may be found in References [3,4,13,16,17,18,19,20,21,22,23,24]. The effect of Reynolds number is very strong in the region of transition [4,18].

Installing transition strips may cause reduction of the side force by as much as 80%, causing early transition to turbulent boundary layer at low Reynolds numbers. (Surface roughness has a similar effect).

(5) Also free stream turbulence does influence the magnitude of the lateral forces and moments acting on a body, (Ref. 67). Therefore, results from wind tunnel tests may vary to a significant extent, depending on the tunnel free stream turbulence level.

Several works try to give a model to predict the position of separation, the asymmetric vortex structure and the forces and moments acting on slender bodies at high angles of attack. (For example. Refs. 9, 16, 25, 26, 27, 28, 29, 30, 31, 32, 33, 34). As stated in Ref. 35, the success of these methods is only partial, and the theoretical state of the art

for calculating steady asymmetric vortex patterns around bodies of revolution at low speeds is semi-empirical. At present only engineering methods of limited range of applicability are available.

2.2. Methods for the Suppression and Control of the Side Force and Yawing Moment at High Incidence in Zero Side-Slip.

Side forces and moments may be potentially hazardous to the control and stability of slender configurations such as modern fighters and missiles maneuvering at high angles of attack. These side forces and moments may be overcome by sufficient control authority, or by aerodynamic devices which suppress the asymmetric vortex pattern.

The most common aerodynamic devices used for side force alleviation are transition strips of all kinds [10,11,15,17,36] and vortex generators such as small strakes usually placed on the forebody or near the nose [12, 13,14].

A method for active control of asymmetric vortex effects is presented in Ref. 37, using rotation of portions of the body about the axis.

Another device for control of forebody vortex orientation is presented in Ref. 38, where tangential blowing to the body surface in small amounts, helped to alleviate lateral forces and moments, and even to control them to some extent. A control device is proposed for future investigation. Effects of normal blowing of small jets on lateral forces and moments are described in Ref. [1-4] and also in Refs. [39,40,41], where it is shown that effective alleviation of side force and yawing moment is achieved with relatively small amounts of blowing. An extended summary of the phenomena devices described in this chapter appears in Ref. 21.

It should be noted that some of the devices described above do suffer from certain defaults. In some cases the use of transition strips reduced side forces but also affected the normal force and pitching moment causing early "stall" effects. Strakes seem to be effective in alleviating side forces only in a certain limited range of angles of attack. In general, the role of these devices is a passive one, and apart from alleviating side forces, these devices could not be used for active lateral control of side forces and yawing moments at high angles of attack, for the benefit of improved maneuverability. Some of the other devices presented before seem to be too complicated for use.

The present research effort is a continuation of the investigation on the effect of air jets blown from the nose of a body of revolution for the alleviation and also for the control of side forces and yawing moments at high angles of attack, in subsonic and transonic Mach numbers (previous results are reported in Refs. 1-4).

2.3. Studies of Side Force and Yawing Moment Alleviation and Control on a Cone-Cylinder Body at High Angles of Attack, Using Small Symmetrical Jets Injected From the Nose at Subsonic and Transonic Mach Numbers

2.3.1. The Model and the Experimental Facilities

The experiments are conducted in the Subsonic Wind Tunnel of the Aeronautical Research Center of the Technion with a cross section of 1m x 1m, and in the Transonic Wind Tunnel (blow down, induction type), with a cross section of 0.8m x 0.6m. The model shown in Fig. 1 is 3cm. dia. cylindrical body having an overall finesse ratio of 6. The

nose of the body is a pointed cone, with length/diameter ratio of 2.

Using the results of previous experiments [1,2], it was decided to concentrate the tests on a sharp cone forebody, and to inject the air jets from a station which was close to the nose apex at angles of -30° to the horizontal plane of the body. This location of the pair of holes for injection gave the best results in the previous tests.

Some tests results are presented here also for $+30^{\circ}$ angle of injection for comparison purposes. The diameter of the holes is 1.2mm each, perpendicular to the body axis of revolution. (The diameter of the holes is chosen so as to obtain blowing velocities of the same order of magnitude as the tunnel flow speed).

A system of rigid and flexible tubing is arranged in the model so as to supply the air for symmetrical blowing. A special device was developed and built, which enables continuous change of the rate of blowing and its measurements, so that the rate of blowing is directly recorded by the computer together with all other data readings during the experiments. Internal strain gage balances are used to measure the aerodynamic forces and moments. The balance chosen has particularly sensitive elements for the measurements of side forces and yawing moments. Visualization tests are performed using oil-flow at low subsonic speeds and Schlieren photography at high subsonic and at transonic Mach numbers. Visualization tests are carried out with and without injection, for comparison of the flow patterns. Tests with and without injection are repeated so as to verify the repeatability of the results.

Special measures are taken in the model installation to assure that the same angular position of the cone and the cylinder in each experiment is obtained in the tunnel so as to prevent any changes in the side force direction and magnitude due to variation in model installation.

The symmetry of the blowing jets is checked by blowing with no external flow and detecting zero lateral forces and moments.

2.3.2. Results

(a) Low Subsonic Tests

The low subsonic tests are carried out at 32m/sec. in an angle of attack range of -10° to 90° . Comparison is made between tests without a transition device, and tests with a transition strip (ring) of 0.1mm thickness placed at $x/d = 0.333$ from the nose tip. The thickness and location of the transition ring are chosen according to Refs. 42, 43. The effect of the jet blowing is also tested with the without transition ring.

From Fig. 2 it can be seen that the normal force and pitching moment coefficients are only moderately affected by the transition ring especially near the region of their peak. Normal force peak with a transition ring is about 10-15% less than without transition, while there is only a slight difference between the curves up to 40° angle of attack.

However, Figs 3 and 4 show that the influence of the transition ring is quite large on the side force and yawing moment coefficients. There is a great reduction in the side force and yawing moment, using the transition ring, up to about 56° angle of attack, while peak position for the side force is shifted down to about $\alpha = 41^\circ$ (from $\alpha = 48^\circ$ without the transition ring). The maximum side force coefficient is reduced by 25%, using the transition rings. It is also interesting to note the development of a negative secondary peak of side force, with the transition ring, at about $\alpha = 60^\circ$. Worth noting

is also the fact that without the transition ring the maximum side force coefficient is at $\alpha = 48^\circ$, while the yawing moment peak is occurring at about $\alpha = 40^\circ$. The position of both these peaks occurs at about $\alpha = 41^\circ$ when the transition ring is present. The angle of onset of side forces is unaffected by the transition ring and stays at about 24° .

Effects of Jet Injection on Side Forces and Yawing Moments, with and without Transition Ring, (Injection at -30° to the Horizontal Plane of the Body, Windward).

The effect of jet injection is demonstrated in Figs. 5 and 6 (no transition ring) and in Figs. 7 and 8 (with transition ring). In Figs. 5 and 6 it can be seen that jet blowing from the chosen station on the nose effectively alleviated side forces and yawing moments above $\alpha = 44^\circ$. Blowing is ineffective below $\alpha = 44^\circ$, without a transition ring.

The behaviour of the curve describing the variation of C_y or C_n versus the blowing coefficient C_μ has a special form (when the blowing is effective). It can be seen that there is a sharp reduction in C_y and C_n at a very low blowing rate, and as C_μ grows there is a change of sign, reaching a negative but lower peak (in absolute value). That peak is usually much more "flat" and when C_μ is increased further, a second zero of C_y and C_n may be achieved, sometimes accompanied later by a second positive peak at high blowing rates. The very sharp change in C_y and C_n at very low blowing rates might be caused by the jets, which act to trip the boundary layer. This possibility is supported by some oil flow visualization photographs, in which there is a distinct curved

pattern starting from the injection holes, rolling up along the conical nose, up to the shoulder, or to the nearest separation lines. However, Figs. 22, 23 which are examples of the oil flow visualization photographs show that the small jets also affect the symmetry of the separation lines along the leeward side of the body. The effect of the jets on the boundary layer transition is clear also from their influence on C_{NOR} especially at high angles of incidence (Figs. 9, 10).

When a transition ring is present, (Figs. 7 and 8), the sharp change in C_Y and C_n disappears at $\alpha = 32^\circ$ and 36° , and starts appearing again at $\alpha = 40^\circ$ up to about 58° . This can be explained by the fact that the small transition ring is more effective at the lower range of angles of attack in reducing side forces, but it is less efficient at the higher angle of attack range, where the cross flow plane becomes more dominant, and there the effect of the jets is stronger.

Fig. 10 supports this view, where the normal force is unaffected by the jets at $\alpha = 32^\circ$, 36° with a transition ring, and starts being affected at higher angles of incidence.

The influence of injection apart from transitional effect is clearly demonstrated in Fig. 22, where the transition ring is present, and the angle of incidence is 40° . Here the injection completely alters the separation pattern, apart from making it more symmetrical. The pair of separation lines on the leeside of the cone which continues over the shoulder along the cylinder without injection, breaks at the shoulder when injection is present, and a new pair of separation

lines appears on the cylinder. The shoulder between the cone and the cylinder has been observed to have its own effects on the flow pattern, some of which are weaker or non-existent in models such as ogive-cylinder bodies. It should be noted that in the last case a higher blow rate was used for side force alleviation than in "transitional" cases (See Fig. 7 for $\alpha = 40^\circ$).

The amount of flow rate coefficient needed for side force alleviation vs. the angle of incidence is sketched in Fig. 11.

It is clear that high blowing rate is needed at the lower range of α , up to about 46° : 48° . Then there is the range of α (48° to 58° with transition ring, or 48° to 64° without it) where very low blowing coefficient is needed to eliminate even high side forces. The last range corresponds to the negative slope region of C_y vs. α (Fig. 3).

The sharp rise in the required blowing coefficient at $\alpha = 60^\circ$ (with transition ring) coincides with the negative peak of side force (Fig. 3), and the amount needed for side force alleviation is almost the same as that needed to alleviate the side force of the same positive amount at $\alpha = 40^\circ$. (The border lines which appear in Fig. 11 for some values of α indicate the region of blowing rates in which side force is effectively zero or strongly alleviated). When analyzing Fig. 11, one should remember that this figure shows only a typical behaviour for the case of windward blowing, since the level and even the shape of the curve might change to a certain amount, should any difference occur in the model mounting or orientation, between tests. This is also connected with the fact that the amount of jet blowing

needed for side force alleviation depends not only on the angle of incidence but also on the amount of the side force to be alleviated.

Effects of Circumferential Position of Injection

Although this parameter has already been studied [1,2,41] to some extent, we choose to present some more results about this subject, which seem important when trying to understand the mechanism of jet influence on the flow. For comparison, results are presented for two injecting circumferential positions:

- (a) Injection at -30° to the horizontal plane of the body, (windward) which is the station chosen for most of the tests (see Fig. 1), because of the relative low-amounts of injection rate needed for side force alleviation.
- (b) Injection at $+30^\circ$ to the horizontal plane of the body (leeward), a position which is obtained in the present case by rotating the body 180° on its axis of revolution.

(In both cases no transition device is present).

Fig. 12 gives the variation of side force coefficient vs. angle of attack for different amounts of jet blowing for the windward and leeward cases. Note the good repeatability of the results in the two cases, between the basic curve and the curve of $C_\mu = 0$, (obtained in separate tests). Because of the difference of roll angle between these two cases, there is a notable difference in the level of C_y and its general behaviour vs. angle of attack, as expected. Therefore the comparison between the windward and leeward cases should be done carefully. Comparison is done by presenting the amount of C_μ needed for side force alleviation for various angles of attack, (Fig. 13) and

by presenting also the amount of C_{μ} needed for side force alleviation for various amounts of side force coefficients, C_Y to be alleviated (Fig. 14). An additional, separate test run is presented in both figures, for injection at -30° (windward) for a slightly different model mounting, which encountered higher side forces. It is interesting to note that in any case the amount of jet blowing needed is in most of the domain far lower (Figs. 13 and 14) for windward injection at -30° , than in the case of leeward injection at $+30^\circ$. However, it is also clear that leeward injection at $+30^\circ$ successfully alleviated all side forces at angles of attack even below 44° , a domain in which windward injection at -30° was almost ineffective without a transition strip. The amount of C_{μ} needed for side force alleviation in this domain is relatively very high. Leeward injection alleviated consistently both C_Y and C_n in all cases, while (in some few cases) windward injection alleviated only C_Y . This points to a probable difference in the mechanism of influence between the cases, and it seems that each of the injection cases has a domain of angles of attack in which it is more efficient than the other. This is not surprising when looking at the effect of angle of attack on the flow character at a given Reynolds Number, as reported by Refs. [3,4] and especially by Ref. [18]. At a given Re_D number, increasing α may clearly change the character of the flow causing a change from turbulent separation to transitional separation or from transitional separation to laminar separation in some cases of low Re_D . The rate of injection and the circumferential angle of jet injection efficiency depends very much on the character of the flow around the body.

(b) High Subsonic and Transonic Speeds Tests

The effect of Mach number at two fixed angles of incidence, $\alpha = 46^\circ$, $\alpha = 48^\circ$, is shown in Figs. 15, 16. The rise in C_{NOR} and the equivalent change in C_M because of Mach number effect starts at about $M = 0.63$.

It is interesting to see that both side force and yawing moment change their sign around $M = 0.7$, because of Mach number effects. (The reason might be connected with the first appearance of shock waves at that Mach Number). The C_Y and C_n curves then reach an unstable peak between $M = 0.77$ and $M = 0.92$. This result is different from the conclusions presented in Ref. 14 which states that side forces on body of revolution are reduced to zero for crossflow Mach number greater than about 0.5.

It can be seen (Fig. 16) that there is a great reduction in the side force and yawing moment when the Mach number exceeds $M = 0.92$. (Equivalent cross flow Mach number is about 0.66).

Fig. 27 shows the development of the flow as the Mach number grows from 0.4 to 1.1, using Schlieren photographs.

The variation of C_Y and C_n vs. the angle of incidence at various Mach numbers is shown in Figs. 17, 18. Noteworthy is the sharp change in C_Y and C_n at $M = 0.4$, from a mild positive peak to a sharp negative peak, and then again to a mild positive peak. The reason might be connected with vortex breakdown. In general, the side forces and yawing moments above $M = 0.4$ are about 4 or 5 times less than at $M = 0.1$, and the reason is that the flow becomes fully turbulent, together with possible vortex breakdown phenomenon. (See also discussion of Reynolds number effect).

The Effect of Jet Blowing at High Subsonic and Transonic Mach Numbers

The effect of windward jet blowing at -30° on C_Y and C_n is presented in Figs. 19 to 21.

The rates of jet blowing coefficient become quite small as the Mach number increased, so its effect is only partial.

At $M = 0.4$ (Fig. 19) jet blowing is ineffective at $\alpha = 46^\circ$ and causes an unstable change in C_Y and C_n at $\alpha = 48.5^\circ$. This is explained by results shown in Figs. 17, 18, where a sharp slope in C_Y and C_n is observed in this region.

At $M = 0.7$ (Fig. 20) there is a considerable alleviation of C_Y and C_n at $\alpha = 37.5^\circ$, but the blowing causes higher C_Y and C_n at $\alpha = 46^\circ$, where the side force is initially close to zero.

Schlieren photographs taken at $\alpha = 37.5^\circ$ and at this Mach number with and without injection reveal some information about the effect of jet blowing in this case. It can be clearly seen in Fig. 28 that the main line of separation at the nose is broken near the shoulder of the cone without injection, (possibly because of the small shock line starting at this point). Secondary separations are observed further on the cylindrical part. However, with the blowing it can be seen that a distinct vortex is separated from the nose, trailing high above the cylinder part and not broken in the shoulder region. Secondary separations are still observed on the cylinder.

At $M = 0.85$ (Fig. 21), jet blowing at $\alpha = 47^\circ$ managed to alleviate C_Y , but only reduced C_n . No effect of jet blowing at this rate is noted at $M = 1.0$.

One also should remember that at transonic Mach numbers, where shock waves are involved, there might be a stronger importance to the position of the jet blowing stations.

The effect of the small rate of jet blowing at transonic and high subsonic Mach numbers is noteworthy (when existent). Clearly the effect is not due to transition of the boundary layer because of the already high Reynolds numbers, and tunnel noise level. The Schlieren photograph of Fig. 28 clearly reveals that it has to do with vortex separation and breakdown. (The fact that jets can inhibit vortex breakdown is already known).

(c) Reynolds Number Effect

Fig. 22 shows the effect of Reynolds number on C_{NOR} and C_y , at various angles of attack. It is clear that there is a strong transition effect of Re_D on these forces, at all angles of attack, causing a sharp drop in C_{NOR} at higher Reynolds numbers which explains the lower C_{NOR} for a given α at $M = 0.4$, compared to the $M = 0.1$ results. At higher angles of incidence the variation of the C_{NOR} is somewhat similar to the variation of the drag coefficient (and indeed at those angles a large portion of the C_{NOR} is due to the drag). The behaviour of C_y is very interesting.

It is clear that there is a sharp change of sign in C_y in the transitional region, and then a more moderate rise, changing sign again at a higher Re_D . These results show clearly that the direction of side force might be changed because of Reynolds number effects in the transition region. Therefore under such conditions the side force may not stay in its original direction as some investigators suggested. (In this connection see also Refs. 17, 18, 24, 33). The results

presented here are strongly supported by Ref. 18, where the flow regimes (Laminar, Transitional and Turbulent) are fully analysed and mapped as a function of Reynolds number and the angle of incidence.

Figs. 23 and 24 show the effect of Reynolds number on the pitching moment and on the yawing moment coefficients. The variation in the pitching and yawing moments at various Reynolds numbers indicate that unstable behaviour of the model may occur at high angles of attack, requiring special attention in the control considerations of these designs at certain ranges of speeds and altitudes. In view of these phenomena, blowing of jets may be a useful method for stabilization and control at such flight conditions.

3. A METHOD FOR THE CALCULATION OF THE LONGITUDINAL AERODYNAMIC CHARACTERISTICS OF BODIES AT ANGLES OF ATTACK, INCLUDING SYMMETRIC VORTEX SEPARATIONS IN SUBSONIC FLOW.

3.1. State of the Art

Most of the existing methods for calculating aerodynamic forces, moments and pressure distributions over bodies and wing body configurations use non-lifting potential elements. In those methods point sources and source panels are used in order to satisfy the thickness distribution of the body. Refs. [48, 49, 50, 51, 52, 53]. Some methods try to use the quadrilateral vortex ring for the description of the body as an "annular wing", Refs. [54, 55, 56]. The regular vortex lattice is also used for the description of the body as an annular wing Ref. [57] and the work of Miranda in Ref. [56]. Combinations of source panels and vortex rings are also used, Refs. [55, 58], and other combinations are used for the description of thick wings, Refs. [48, 50, 51, 54, 59, 60, 61]. (The references given here are only an example for the various basic methods and not a full reference review). The main problem with the methods described above is the fact that although describing 3-d bodies, they do not allow for vortex flow separations from the surface of the body at angles of attack, therefore, their results are limited to very low angles of attack. There are some methods that try to give a model for the separation of vortices from bodies at incidence. Most of these methods use the cross-flow theory model for the calculations Refs. [27 and 30] so that their results are relevant to very slender bodies. Ref. 28 presents a more complicated method for calculating the separation of flow from bodies at incidence, introducing also viscous considerations for the boundary layer and for the diffusion

of the vortex wake. The model is rather complicated and is based on a transformation of the 3-d steady flow equations to 2-d, non-steady cross-flow equations. The required computer resources for the last case are rather high. All the methods described use some empirical information at least as to the location of the points of separation. Ref. 62 presents a method which combines the potential solution for a body at incidence with a superimposed wake composed of vortex filaments. The model makes use of empirical data for the wake, together with cross flow theory considerations, and in this ~~sense~~ its consistency is incomplete.

It is clear that the existing methods are not sufficiently developed for the calculation of aerodynamic characteristics of bodies and of wing-body configurations at incidence, when vortex separations in 3-d flow occur.

3.2. The Proposed Computational Method for Incompressible Flow.

A relatively simple model has been developed for the description of slender bodies at incidence. The model consists of two elements:

- (1) Potential sources/sinks for the solution of the basic thickness problem at zero angle of attack. Point sources on the axis of revolution are used for axisymmetric slender bodies, and source panels may be used for bodies which are not slender or which are not axisymmetric.
- (2) Vortex lattice cells are spread on the body surface, for the representation of the lifting case at non zero angles of attack. The vortex lattice is super-imposed on the source

field. (See Fig. 29 as an illustration for the model).

The process of solution is as follows:

(a) The strength of the sources is calculated at zero incidence to evaluate the thickness function. A geometrical influence matrix $[H]_0$ is calculated first for unit strength sources and at control points on the body surface (which coincide with the control points of the vortex lattice cells which are used for the lifting case calculations). The solution for the strength of the sources is obtained by imposing the condition that there will be no net flow through the body surface at the control points, which means that the velocity induced by the sources at the control points should balance the normal component of the free stream velocity $\{v_n\}_0$ at these points. The strength of the sources $\{s\}_0$ is then the solution of the linear system.

$$[H]_0 \cdot \{s\}_0 = -\{v_n\}_0 \quad (1)$$

(b) The body is now placed at an angle of attack α . A new matrix of influence coefficients $[H]_\alpha$ is evaluated for the influence of unit strength horse-shoe vortices spread on the body, on the control points of the mesh using Biot-Savart law. The normal component of the free stream velocity $\{v_n\}_\alpha$ is recalculated at each control point. Initial conditions for the vortex wake and separation points are also taken into account when constructing the influence coefficient matrix. The vortex system compensates only for angle of attack effect, so that the strength of the bound vortices $\{k\}_\alpha$ is obtained by solving the linear system of equations:

$$[H]_{\alpha} \cdot (K)_{\alpha} = -[\{v_n\}_{\alpha} - \{v_n\}_{\infty}] \quad (2)$$

(c) After solving for the strength of the bound vortices, the induced velocity components (u, v, w) of the whole field of sources and vortices are calculated at each control point, and the pressure coefficient at each point is also calculated by the expression:

$$C_p = 1 - [(U + u)^2 + v^2 + w^2]/U^2 \quad (3)$$

The overall aerodynamic coefficients are calculated then by the following expressions:

$$C_L = \frac{4}{US_{ref}} \sum_{j=1}^{N_s} \{ \sum_{i=1}^{N_c} [(1 + \frac{u}{U} - \frac{v}{U} \frac{\Delta x}{\Delta y}) \cdot K]_{ij} \Delta y_j \} + \\ + \frac{-4}{US_{ref}} \sum_i \sum_j (\frac{v}{U} \cdot \Delta K \cdot \Delta x)_{ij} \quad (4)$$

Here $(x, y, z)_{ij}$ are the Cartesian components of a bound vortex segment ij in the direction of x, y, z accordingly, while $(u, v, w)_{ij}$ are the disturbance velocity components at the point of force calculation. The second term on the right hand of Eq. (4) is the contribution of in-surface trailing vortices to the lift, expressed in a general form. This term should not be ignored when considering the relatively large velocity disturbances and the accumulation of trailing vortex strength in bodies. The induced drag coefficient is:

$$C_{Dl} = \frac{-4}{US_{ref}} \sum_{j=1}^{N_s} \sum_{i=1}^{N_c} [(\frac{w}{U} \Delta y + \frac{v}{U} \Delta z) K]_{ij} + \\ + \frac{-4}{US_{ref}} \sum_i \sum_j [\frac{v}{U} \Delta K \cdot \Delta z + \frac{w}{U} \Delta K \Delta y]_{ij} \quad (5)$$

and the pitching moment coefficient is:

$$C_M = \sum_i \sum_j C_{L_{ij}} \cdot \frac{(x_{ij} - x_{ref})}{C_{ref}} + \sum_i \sum_j C_{D_{ij}} \frac{(z_{ij} - z_{ref})}{C_{ref}} \quad (6)$$

x_{ref} and z_{ref} are x and z coordinates of the pitching moment reference point. The second term on the right hand-side of Eq. (6) expresses the contribution of induced drag to the pitching moment, which is usually ignored at low angles of attack. The center of pressure is given by

$$x_{CP} = - \frac{C_{ref} \cdot C_M}{C_L} \quad (\text{measured from } x_{ref}). \quad (7)$$

In general it should be noted that some of the assumptions made when neglecting terms like those containing the effect of side-wash, prove to be incorrect when dealing with the strong velocity disturbances induced by 3-d bodies, and with the presence of rather strong trailing vortices.

An alternative to the expression given before for the calculation of the aerodynamic coefficients is to calculate them using the pressure coefficient $C_{P_{ij}}$ at each cell ij . If ΔS_{ij} is the area of cell ij and $n_{ij} = (n_x, n_y, n_z)_{ij}$ is the normal to the surface of cell ij then

$$C_L = \frac{1}{S_{ref}} \sum_i \sum_j (C_P \cdot \Delta S \cdot n_z)_{ij} \quad (8)$$

$$C_{D_i} = \frac{1}{S_{ref}} \sum_i \sum_j (C_P \cdot \Delta S \cdot n_x)_{ij} \quad (9)$$

$$C_M = \frac{1}{S_{ref}} \sum_i \sum_j [C_P \Delta S n_z]_{ij} \cdot \frac{(x_{ij} - x_{ref})}{C_{ref}} - \frac{1}{S_{ref}} \sum_i \sum_j [C_P \Delta S n_x]_{ij} \cdot \frac{(z_{ij} - z_{ref})}{C_{ref}} \quad (10)$$

(d) The velocity and the pressure field are examined, and separations of the trailing vortices are allowed (See illustration in Fig. 29) whenever the criterion for separation is satisfied.

The separated vortices undergo an iterative calculation to determine their path according to the boundary condition for the wake. That is, in the wake the vortices are free and do not carry any forces. Each free vortex is divided into segments, and each point (i) belonging to the tip of a segment is moved according to Euler's method of integration:

$$y_i^{(2)} = y_{i-1}^{(2)} + \frac{v_i^{(1)}}{U + u_i^{(1)}} \Delta x \quad (11)$$

$$z_i^{(2)} = z_{i-1}^{(2)} + \frac{w_i^{(1)}}{U + u_i^{(1)}} \Delta x \quad (12)$$

Here $u_i^{(1)}$, $v_i^{(1)}$, and $w_i^{(1)}$ are the Cartesian components of the induced velocity at point (i) before moving it. $y_i^{(2)}$ and $z_i^{(2)}$ are the new y and z coordinates of point (i). More sophisticated integration methods may be applied at a considerable expense of computer resources. The integration process continues iteratively until the path of the vortices is converged, or until a pre-fixed number of iterations is exceeded.

It should be noted that the body bound vortices and the free vortices are treated as one system, and that they influence each other, and so this method presents a fully consistent model. The basis for this model appears in the 3-d wing/wake calculations, Refs. [63, 64, 65].

(e) The influence coefficients matrix $[H]_{\alpha}$ is now recalculated, and the whole process starts again until convergence of the calculated values for the aerodynamic coefficients is achieved. The calculated vortex wake values after each calculation serve now as an initial condition for a new iteration. Fig. 30 describes a flow chart of the method.

3.3. Results of Calculations

3.3.1. Computational Aspects and Problems

Preliminary work with a model of a body consisting of vortices alone does not give a good description for the body. The reason for this is that the main problem (especially at low incidence) is a thickness problem, and horse shoe vortices alone cannot account for such a problem. However, it seems also that especially in cases of pointed nose bodies, the description of the body by potential sources alone is inaccurate to some extent even at zero angle of attack. The reason for this is that sources alone cannot describe pointed noses close to the apex. The best results for such a case are achieved when after the first calculation of sources strength, vortices together with at least one new source are superimposed to describe the angle of attack effect. The new source is placed close to the nose tip, so that both local slope and no penetration condition through the nose apex are satisfied at this sensitive region. In this manner pressure distribution results for the relatively difficult case of a cone cylinder are greatly improved near the nose tip. It is also interesting to note that when applying this idea, bound vorticity is obtained on the body surface even at zero angle of attack due to nose effect. The strength of this bound vorticity decreases sharply from the nose tip downstream. No net vorticity

is shed in this axisymmetric case and the bound vorticity in this case is formed in rings. Another improvement in the axial pressure distribution is obtained using a variable mesh size at sensitive regions like the nose apex and shoulders of the body. At non-zero angle of attack it is found that the bound vorticity strength varies from cell to cell, causing the pressure distribution to vary both axially and circumferentially. Definite regions of minimum pressure are formed in the crossflow planes and also in axial direction. It is also interesting to note that the strength of the trailing vortices which are imbedded in the surface appear to be of the same order of magnitude as that of the bound vortices at some stations, due to their accumulation along the body. This is an indication that when such a trailing vortex is separated, it may be quite strong. At present the criterion for separation of free vortices from the surface of the body is close to the location of points of minimum pressure coefficient C_p . Since the model is inviscid, this is the most simple and obvious criterion to choose. It is assumed that the flow cannot resist an adverse pressure gradient behind such a point. This criterion is found to be quite realistic at least for the main vortex separation (see Experimental Results of Ref. 41). Another aspect that restricts the amount of refinement of the criterion for separation is the finite and sometimes quite rough mesh size, and so it seems that the criterion of minimum C_p values could be satisfactory in the first approximation. It should be stressed also that this criterion concerns also axial flow and it is not necessarily a 2-d one. Preliminary calculations show that at low and at medium angles of attack there is a distinct pattern of minimum C_p values along the body without separation, and this pattern

reminds very much of the separation pattern calculated by Ref. 28 at such angles of attack (for an ogive cylinder). However, the position of the minimum value of C_p , (although distinct) is less sharp than that found in experiments since there is no separation involved in these preliminary calculations. A very distinct sharp "peak" in the C_p variation is reported to exist in the model of Ref. 62, but there the model depends very much on the empirical data used for positioning the separation, while the wake is independently evaluated so that it is difficult to "correct" the problem of exaggerated peaks in such a model. It should be stressed that although separation itself is dominated by a viscous mechanism, the pressure distribution that "builds" itself with increasing incidence is mainly a potential phenomena at least up to the point when separation occurs, and thus it provides a consistent criterion for determining the approximate separation point. When trying a model that allowed total vortex separation (from each cell) on the leeside of the body, the method diverged and strong instabilities occurred in the free vortex path calculations. It seems that such an "exaggerated" separation does not fit the real physical phenomenon.

Another problem is the representation of the base flow especially in cases of a blunt or cut-off base. The pressure distribution is influenced by the rear flow, but this influence is decaying fast towards the nose of the body, so that if the body is slender enough the effect is small. In cases of cut-off bases it is found that artificially closing the body by a reasonable shape surface improves the calculated pressure distribution in the rear and along the body. Another yet unanswered question is the correct position of control points in each cell. Whereas in cases of rectangular or even trapezoidal shaped horse show vortices with chordwise trailing vortices the 3/4 rule seemed to yield very satisfactory results, it is not

obvious at all that this is also the best location for body lattice where the "arms" of the horse-shoe vortices are "opening" or "closing" according to the body shape. Trying other criteria for locating the control points (see Ref. 55 for example) is no more than a numerical experiment at most, when there is no analytical basis for it.

3.3.2. Preliminary Results Compared to Experimental Data and to other Analytical Methods.

Fig. 31 shows the pressure distribution on a sharp cone-cylinder body at zero angle of attack. The results of the present calculation are compared to those obtained by Ref. [53] and to experimental results. A mesh that contained only 20 divisions for the cone, and 15 for the cylinder (axial direction) and 6 circumferential divisions, gave very good comparison to the experimental data and to the analytical curve of Ref. 53. (Total number of sources on the axis of revolution is 35). This case is chosen because of the difficulties it presents (sharp nose tip and a discontinuous slope at the shoulder). Circumferential pressure distributions for a tangent ogive-cylinder body at 10° angle of attack, in various stations along the body, using 12 circumferential divisions and 15 axial divisions for ogive, 10 for the cylinder have been compared to experimental data of Ref. 66. There is a reasonable agreement of the pressure distribution for part of the circumferential domain, namely the leeward and windward parts. However, since no separation is involved in these preliminary results, the minimum pressure peak in the vicinity of the shoulder, although distinct it is not as sharp as it appears in the experimental results where separation occurs. This position of the distinct minima is used in the next step to define the position of the separation of trailing vortices, results of which we hope to present in a future report.

4. CONCLUSIONS

4.1. The Effect of Jet Injection on the Lateral Forces and Moments at High Angles of Attack in Subsonic and Transonic Flow

The experimental investigation performed on the cone-cylinder body revealed important features of such configurations at high angles of attack, and their dependence on Mach number and Reynolds number.

At least some of the so called uncertainties in the prediction of the general behaviour of side forces and yawing moments are found to be clearly dependent on these parameters. The strong effect of jet blowing on lateral forces and moments at various Mach numbers and Reynolds numbers has been demonstrated. At low subsonic speed, windward jet blowing may be used efficiently for side force alleviation and even control, especially when a transition ring is present also. Symmetric leeward jet blowing at higher rates is useful too for side force alleviation and control particularly at angles of attack of less than 44° . Jet blowing at small rates is sufficient to alleviate side force in subsonic speeds. At high subsonic and transonic Mach numbers, the rates required for controlling these forces are much larger. Further experiments are needed at the transonic range in order to investigate the effects of parameters such as higher blowing rates and the effects of changes in the blowing stations. More visualization tests can also be useful in order to understand better the various roles of jet injection, in alleviating side forces and yawing moments.

4.2. Calculations of the Flow over Bodies at Incidence in Subsonic Flow, Including the Effect of Symmetric Vortex Separation.

The preliminary results of the present method give encouraging results, even with the rather rough mesh of cells used to describe

the cone-cylinder body. The simplicity of the model makes it convenient for future incorporation in a wing-body analysis. Unlike the other models, the present one is fully consistent in the sense that both the body elements and the vortex wake are treated as one system, including the effects of their interactions. The determination of the separation points is also consistent with the calculations of the pressure distribution of this model. Although the exact location of separation depends also on Reynolds number, it is hoped to get a reasonable first approximation using the criterion of minimum pressure points in the pressure distribution. The preliminary results require further verification in future research of this problem.

REFERENCES

1. Sharir, D., Portnoy, H., and Rom, J., A study of the effects of jets injected from a slender body of revolution on the side forces acting on it at large angles of attack in low speeds, TAE Report. 337, May, 1978, Technion, Israel Inst. of Technology.
2. Rom, J., and Almosnino, D., Studies of non-linear aerodynamic characteristics of finned slender bodies at high angles of attack, TAE Report No. 349, Nov. 1978, Technion Israel Inst. of Technology.
3. Almosnino, D., and Rom, J., Alleviation of the side force and the yawing moment acting on a slender cone-cylinder body at high angles of attack, using small jet injection at subsonic and transonic speeds, TAE Report No. 380, Sept. 1979, Technion, Israel Inst. of Technology.
4. Almosnino, D., and Rom, J., Alleviation of lateral forces and moments acting on a slender body at high angles of attack, using jet injection at subsonic and transonic speeds, AIAA Paper No. 80-1558-CP, August 1980.
5. Werlé, H., Tourbillons de corps fuselés aux incidence élevées, L'Aeronautique No. 79-1979-6, pp. 3-22.
6. Topak, M., and Peake, D.J., Topology of two-dimensional and three-dimensional separated flows, AIAA Paper No. 79-1480, July 1979.
7. Pick, G.S., Investigation of side forces on ogive cylinder bodies at high angles of attack in the $M = 0.5$ to 1.1. range, AIAA Paper No. 71-570, June 1971.
9. Krouse, J.R., Induced side forces on slender bodies at angles of attack and Mach numbers of 0.55 - 0.80, NSRDC Test Rept. May 1971.

9. Thomson, K.D., and Morrison, D.F., The spacing position and strength of vortices in the wake of slender cylindrical bodies at large incidence, Weapons Research Establishment, Salisbury, South Australia, Tech. Rept. NSA 25, June 1969, (also Jr. of Fluid Mech., Vol. 50, Pt. 4, Dec. 1971, pp. 751-783).
10. Keener E.R., and Chapman, G.T., Onset of aerodynamic side forces at zero sideslip on symmetric forebodies at high angles of attack, AIAA Paper 74-770, Aug. 1974.
11. Letko, W., A low speed experimental study of directional characteristics of sharp-nosed fuselage through a large angle of attack range at zero angle of sideslip, NACA TN 2911, March 1953.
12. Clark, W.H., Peoples, J.R., and Briggs M.M., Occurrence and inhibition of large yawing moments during high incidence flight of slender missile configurations, AIAA Paper No. 72-968, Sept. 1972.
13. Skow, A.M., Ttiriga, A., Jr. and Moore W.A., Forebody/wing vortex interactions and their influence on departure and spin resistance, AGARD CP 247, Oct. 1978, pp. 6-1 to 6-26.
14. Coe, P.L., Chambers, J.R., and Letko, W., Asymmetric lateral-directional characteristics of pointed bodies of revolution at high angles of attack, NASA TND-7095, Nov. 1972.
15. Keener, E.P., Chapman, G.T., Cohen, L., and Teleghani, J., Side forces on a tangent ogive forebody with a finess ratio of 3.5 at high angles of attack and Mach numbers from 0.1 to 0.7, NASA TMX-3437, Feb. 1977.
16. Deffenbaugh, F.D., and Koerner, W.G., Asymmetric wake development and associated side force on missiles at high angles of attack, AIAA Paper No. 76-364, July 1976.

17. Przirembel, C.E.G., and Shereda, D.E., Aerodynamics of slender bodies at high angles of attack, *J. Spacecraft*, Vol. 16, No. 1, pp. 10-14, Jan-Feb. 1979.
18. Lamont, P.J., Pressure measurements on a ogive-cylinder at high angles of attack with laminar, transitional or turbulent separation, *AIAA Paper No. 80-1556,-CP*, Aug. 1980.
19. Peake, D.J., Owen, K.F., and Higuchi, H., Symmetrical and asymmetrical separations about a yawed cone, *AGARD CP 247*, Oct. 1978, pp.16-1 to 16-27.
20. Mifsud, L., *Characteristique aerodynamique de corps de revolution munis d'ailes d'allongements divers*, *AGARD CP 247*, Oct. 1978, pp.19-1 to 19-24.
21. Ericsson, L.E., and Reading J.P., Vortex induced asymmetric loads in 2-D and 3-D flows, *AIAA Paper No. 80-0181*, Jan. 1980.
22. Clarkson, M.H., Malcolm, G.N., and Chapman, G.T., A subsonic, high-angle-of-attack flow investigation at several Reynolds numbers, *AIAA Jr. Vol. 16*, No. 1, Jan. 1978.
23. Keener, E.R., Chapman, G.T., Kruse, R.L., Effects of Mach number and after-body length on onset of asymmetric forces on bodies at zero sideslip and high angles of attack. *AIAA Paper No. 76-66*, Jan. 1976.
24. Clark, W.H., and Nelson, R.C., Body vortex formation on missiles at high angles of attack, *AIAA Paper No. 76-65*, Jan. 1976.
25. Lamont, P.J., and Hunt, B.L., Pressure and force distribution on a sharp-nosed circular cylinder at large angles of inclination to a uniform subsonic stream, *J. of Fluid Mech.*, Vol. 76, Pt. 3, pp. 519-559, Aug. 1976.
26. Lamont, P.J., and Hunt, B.L., Prediction of aerodynamic out of plane forces on ogive-nosed circular cylinders, *Jr. of Spacecraft and Rockets*, Vol. 14, No. 1, Jan. 1977, pp. 31-44.
27. Fidler, J.E., Approximate method for estimating wake vortex strength, *AIAA Jr. Vol. 12*, No. 5, May 1974.

28. Marshall, F.J., and Deffenbaugh, F.D., Separated flow over bodies of revolution using an unsteady discrete vorticity cross wake, NASA CR 2414, June 1974.
29. Mendenhall, M.R., and Nielsen, J.N., Effect of symmetrical vortex shedding on the longitudinal aerodynamic characteristics of wing-body-tail combinations, NASA CR 2473, Jan. 1975.
30. Angelucci, S.B., A multi vortex method for axisymmetric bodies at angles of attack, J. of Aircraft, Vol. 8, No. 12, 1971, pp.959-966.
31. Angelucci, S.B., Multi vortex model for bodies of arbitrary cross sectional shapes, AIAA Paper No. 73-104, 1973.
32. Smith, J.H.B., Inviscid fluid models, based on rolled-up vortex sheets, for 3-D separation at high Reynolds number, RAE Tech. Memo. Aero 1738, Nov. 1977.
33. Redding, P.J., and Ericsson, L.E., Maximum vortex-induced side force, Jr. of Spacecraft and Rockets, Vol. 15, No. 4, July-Aug. 1978.
34. Wardlaw, A.B., Jr., Multivortex model of asymmetric shedding on slender bodies at high angle of attack, AIAA Paper No. 75-123, Jan. 1975.
35. Nielsen, J.N., Nonlinearities in missile aerodynamics, AIAA Paper No. 78-20, Jan. 1978.
36. Rao, D.M., Side-force alleviation on slender, pointed forebodies at high angles of attack, AIAA Paper No. 78-1339, 1978.
37. Fidler, J.E., Active control of asymmetric vortex effects, AIAA Paper No. 80-0182, Jan. 1980.
38. Moore, W.A., Skow, A.M., and Lorincz, D.J., Enhanced departure/spin recovery of fighter aircraft through control of the forebody vortex orientation, AIAA Paper No. 80-0173, Jan. 1980.
39. Peake, D.J., and Owen, F.K., Control of forebody 3-D flow separations, Paper 15, AGARD CP-262, May 1979.

40. Peake, D.J., and Owen, F.K., Control of forebody 3-D Flow separations, NASA TM-70593, May 1979.
41. Peake, D.J. Owen, F.K., and Johnson, D.A., Control of forebody vortex orientation to alleviate side forces, AIAA Paper No. 80-0183, Jan. 1980.
42. Braslow, A.L., and Knox E.C., Simplified method for determination of critical height of distributed roughness particles for boundary-layer transition at Mach numbers from 0 to 5, NACA TN 4363, 1958.
43. Stewart, D.G., and Fisher, S.A., Some observations of boundary layer transition on cones at subsonic and supersonic speeds, ARL Note ME 267, 1965.
44. Schwind, R.G., and Mullen, J. Jr., "Laser Velocimeter measurements of slender body wake vortices, AIAA Paper No. 79-0302, Jan. 1979.
45. Clark, W.H., Body vortex formation on missiles in incompressible flows, AIAA Paper No. 77-1154, Aug. 1977.
46. Wardlaw, A.B., Jr. and Yanta, W.J., The flow field about, and forces on slender bodies at high angles of attack, AIAA Paper No. 80-0184, Jan. 1980.
47. Oberkampf, W.L., Owen, F.K., and Shivananda, T.P., Experimental Investigation of the Asymmetric body vortex wake, AIAA Paper No. 80-0174, Jan. 1980.
48. Woodward, F.A., An improved method for the aerodynamic analysis of wing-body-tail configurations in subsonic and supersonic flow, NASA CR 2228 (2 volumes), May 1973.
49. Loeve, W., and Slooff, J.W., On the use of panel methods for predicting subsonic flow about aerofoils and aircraft configurations, NLR Rep. MP 71018.1971.
50. Hess, J.L., Calculation of potential flow about arbitrary 3-D lifting bodies, Rep. AD 755 480, U.S. Dept. of Commerce (Also McDonnell Douglas Corp. Rep. MDC J 5679) Oct. 1972.
51. Rubbert, P.E. and Saaris, G.R., Review and evaluation of a 3-D lifting potential flow analysis method for arbitrary configurations, AIAA Paper 72-188, Jan. 1972.

52. Kraus, W., Panel methods in aerodynamics from "Numerical Methods of Fluid Dynamics" by Wirz and Smolderen, McGraw Hill Publ, 1978, pp.237-297.
53. Hess, J.L. and Smith, A.M.O., Calculation of potential flow about arbitrary bodies, Progress in Aeronautical Sciences, Vol. 8, Pergamon Press, 1966.
54. Maskew, B., Calculation of the 3-D potential flow around lifting non planer wings and wing-bodies using a surface distribution of quadrilateral vortex rings, Loughborough U. of Tech., Rep. TT 7009, 1970.
55. Atta, E., and Nayfeh, A.H., Nonlinear aerodynamics of wing body combinations, AIAA Paper No. 78-1206, July 1978.
56. "Vortex Lattice Utilization," Workshop held at NASA Langley R.C., NASA SP 403, May 1976.
57. Kalman, T.P., Rodden, W.P., and Giesing, J.P., Application of the doublet lattice method to non-planar configurations in subsonic flow, J. Aircraft Vol. 8, No. 6, June 1971.
58. Asfar, K.R., Mook, D.T., and Nayfeh, A.H., Application of the vortex lattice technique to arbitrary bodies, J. Aircraft, Vol. 16, No. 7, July 1979, pp.421-424.
59. Johnson, F.T., Rubbert, P.E., Advanced panel-type influence coefficient methods applied to subsonic flows, AIAA Paper No. 75-50, 1975.
60. Weber, J.A., Brune, G.W., Johnson, F.T., Lu, P. and Rubbert, P.E., A 3-D solution of flows over wings with leading edge vortex separation, NASA SP 347, 1975, pp.1013-1032, Also AIAA Jr. Vol. 14, No. 4, April 1976, pp.519-525.
61. Johnson, F.T., Lu, P., Tinoco, E.N., and Epton, M.A., An improved panel method for the solution of 3-D leading edge vortex flows, NASA CR-3278/3279, July 1980.
62. Sheffield, S.J. and Deffenbaugh, F.D., A 3-D Vortex Wake Model for Missiles at high angles of attack, NASA CR-3208, Jan. 1980.
63. Rom, J., Zorea, C., and Gordon, R., On the calculation of nonlinear aero-dynamic characteristics and the near vortex wake, ICAS Paper No. 74-27, Aug. 25-30, 1974.

64. Almosnino, D., Zorea, C., and Rom, J., A method for calculating longitudinal characteristics of wings and multiple lifting surfaces in subsonic flow, and at high angles of attack, Israel Jr. Tech., Vol. 16, pp.132-141, 1978.
(Proc. XX Israel Ann. Conf. on Aviation and Astronautics).

65. Rom, J., Almosnino, D., and Zorea, C., Calculation of the non-linear aero-dynamic coefficients of wings of various shapes and their wakes, including canard configurations, Proc. XI Cong. of the Int. Council of the Aero-nautical Sciences, Lisbon, Portugal, Vol. I, pp.333-344, Sept. 1978.

66. Tinling, B.E., and Allen, C.Q., An investigation of the normal force and vortex wake characteristics of an ogive-cylinder body at subsonic speeds, NASA TN D-1297, April 1962.

67. Dexter, P.C., and Flower, J.W., Pressures on a Slender, Axisymmetric Body at High Angle of Attack in a very Low Turbulence Level Air Stream, Report No. PCD 8001, Univ. of Bristol, October 1980.

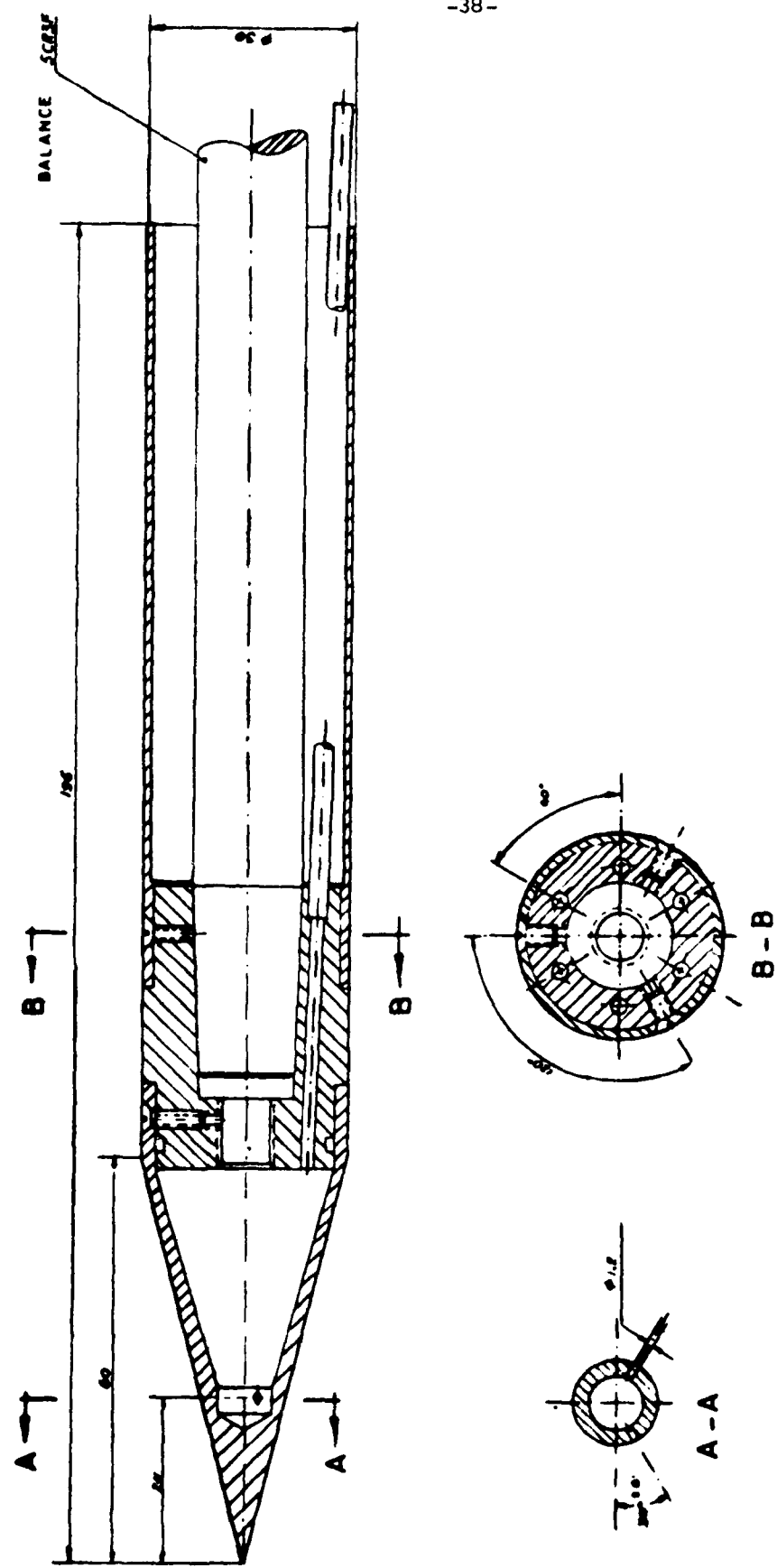


FIGURE No. 1 - THE CONE-CYLINDER MODEL.

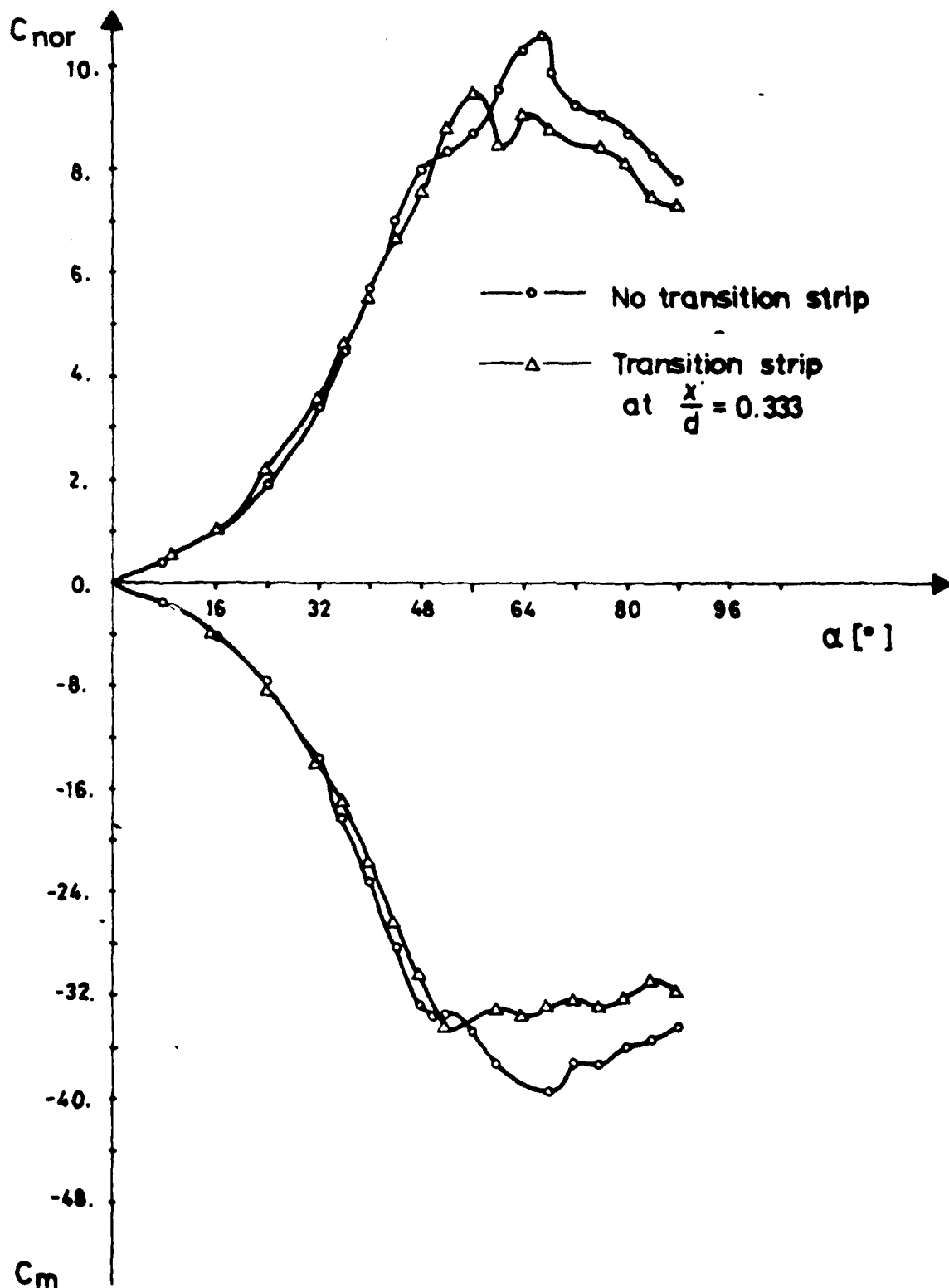


FIGURE No. 2 - NORMAL FORCE AND PITCHING MOMENT COEFFICIENTS VS. ANGLE OF ATTACK, $V = 32$ m/sec, NO INJECTION.

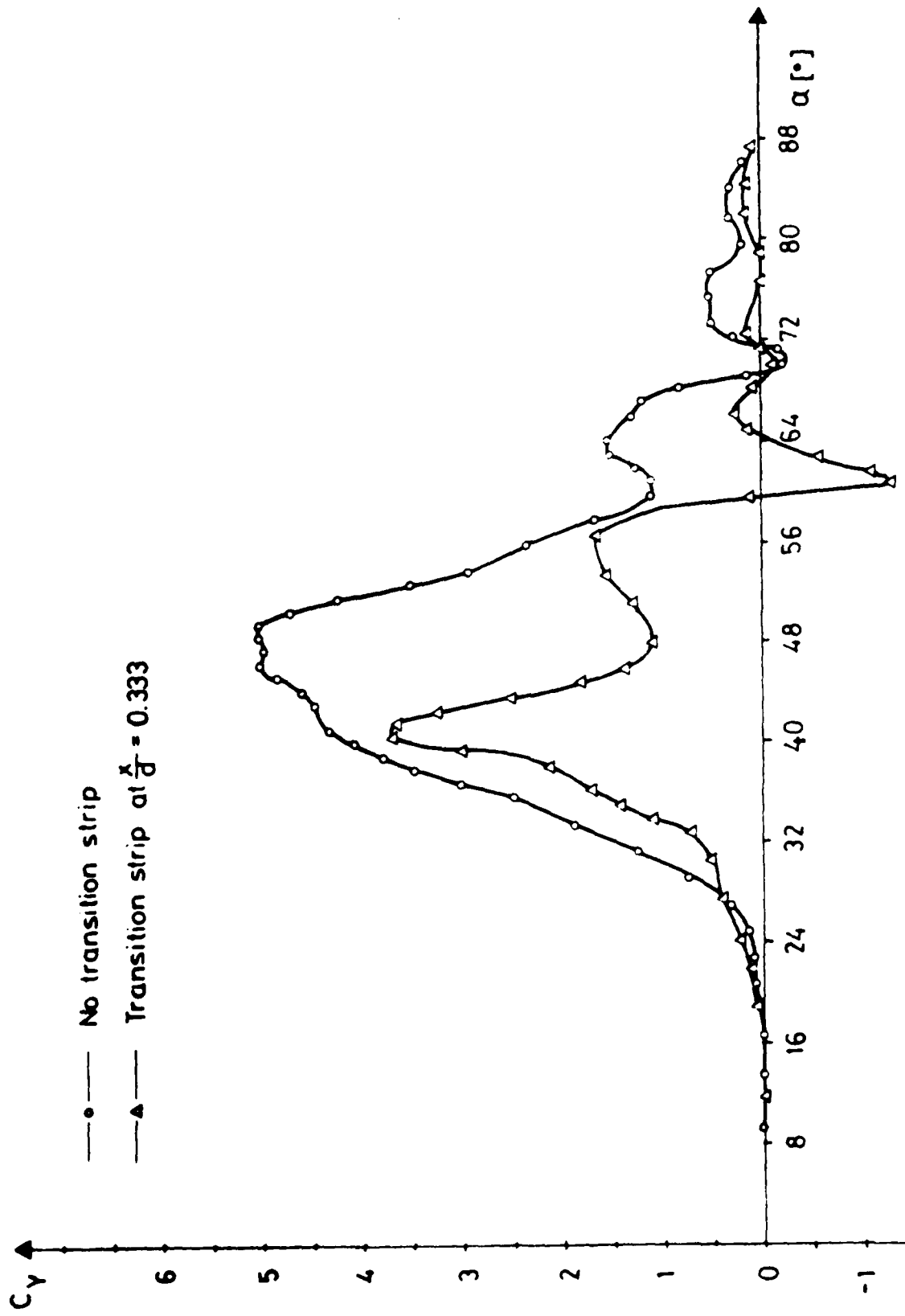


FIGURE No. 3 - SIDE FORCE COEFFICIENT C_y . ANGLE OF ATTACK, $V = 32$ m/sec,
NO INJECTION.

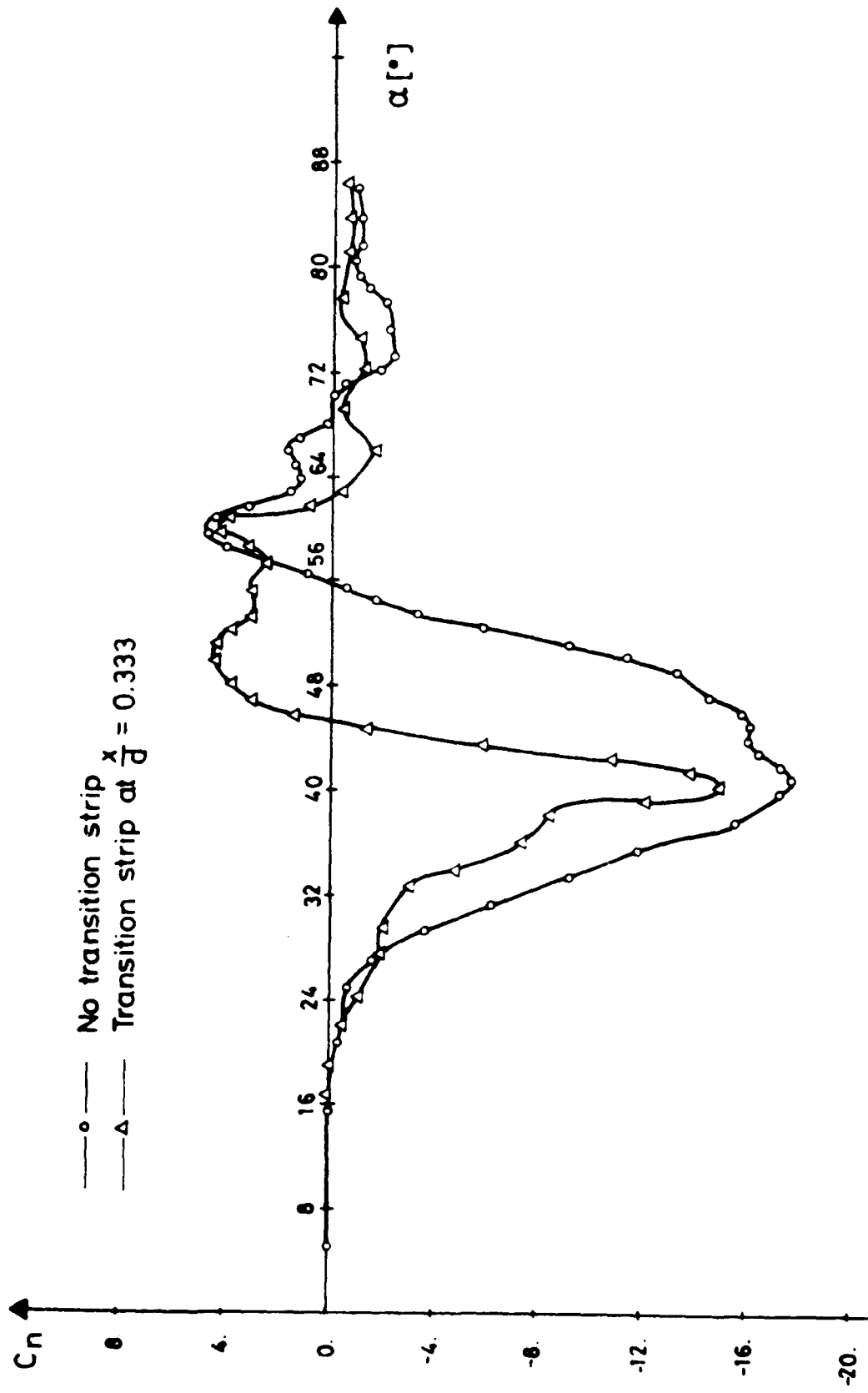


FIGURE No. 4 - YAWING MOMENT COEFFICIENT V_s . ANGLE OF ATTACK, $V = 32 \text{ m/sec.}$
NO INJECTION.

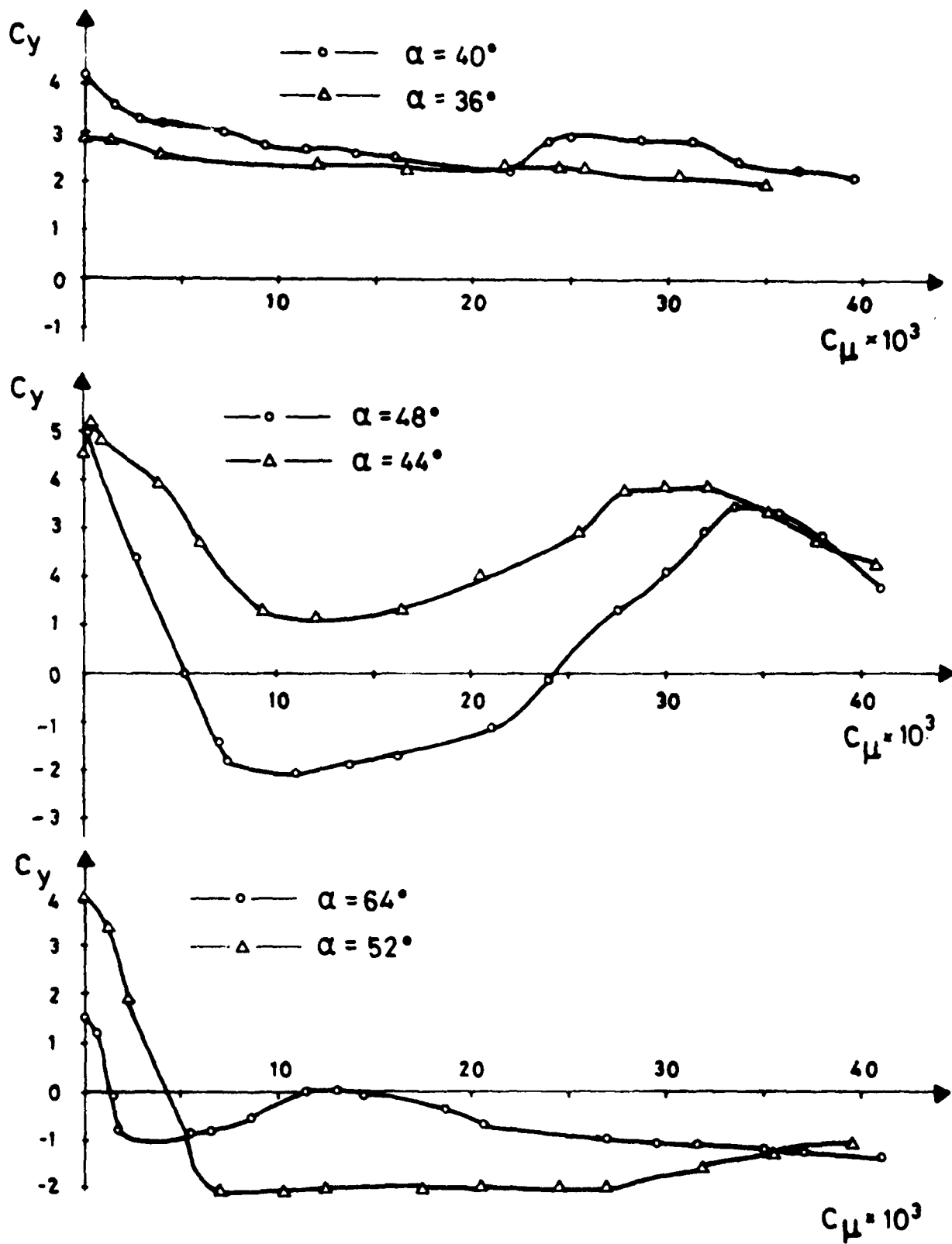


FIGURE No. 5 - VARIATION OF SIDE FORCE COEFFICIENT Vs. BLOWING RATE COEFFICIENT, AT VARIOUS ANGLES OF ATTACK, $V = 32$ m/sec, NO TRANSITION STRIP.

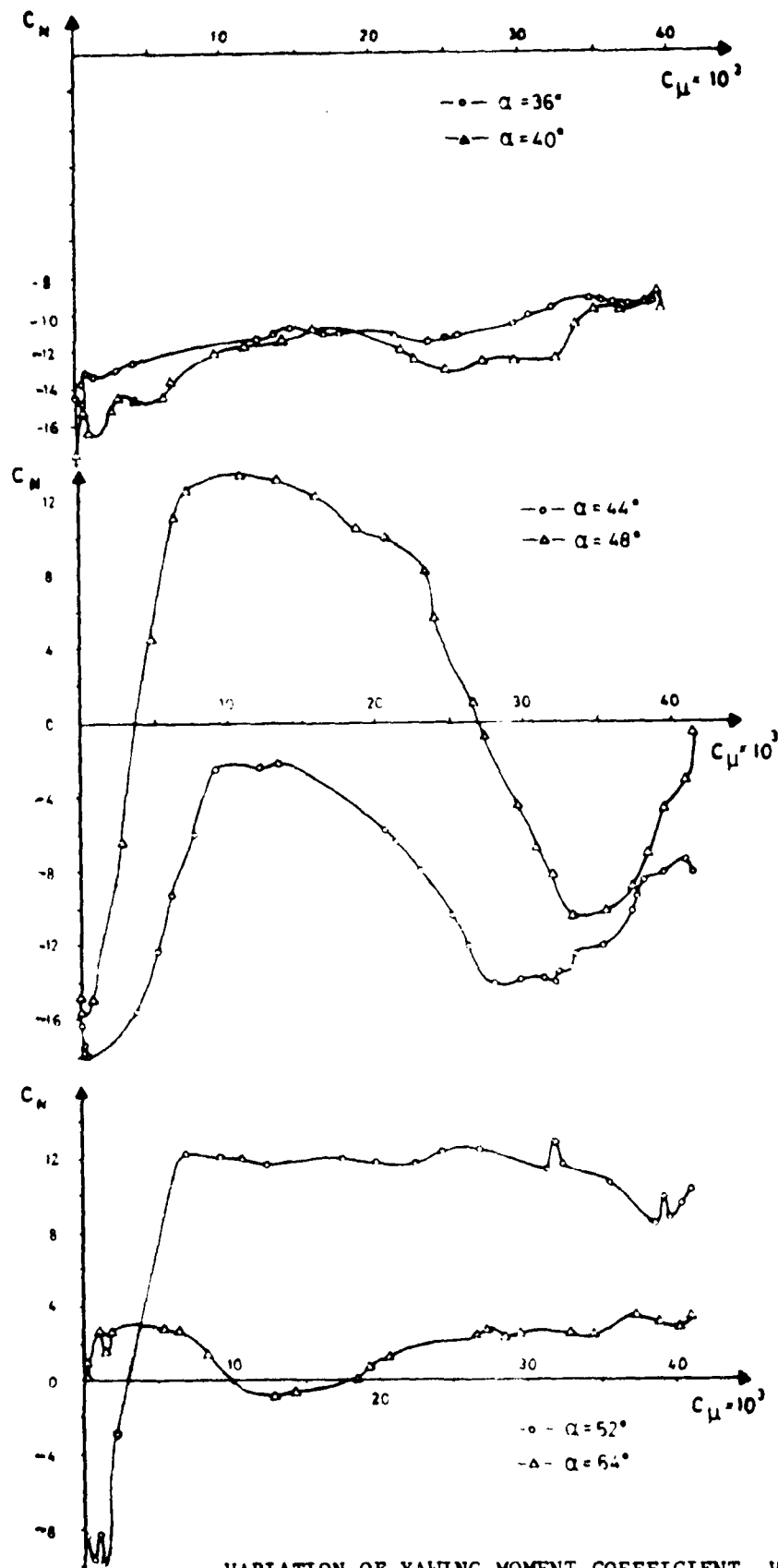


FIGURE No. 6 - VARIATION OF YAWING MOMENT COEFFICIENT Vs. BLOWING RATE COEFFICIENT, AT VARIOUS ANGLES OF ATTACK, $V = 32$ m/sec,
NO TRANSITION STRIP.

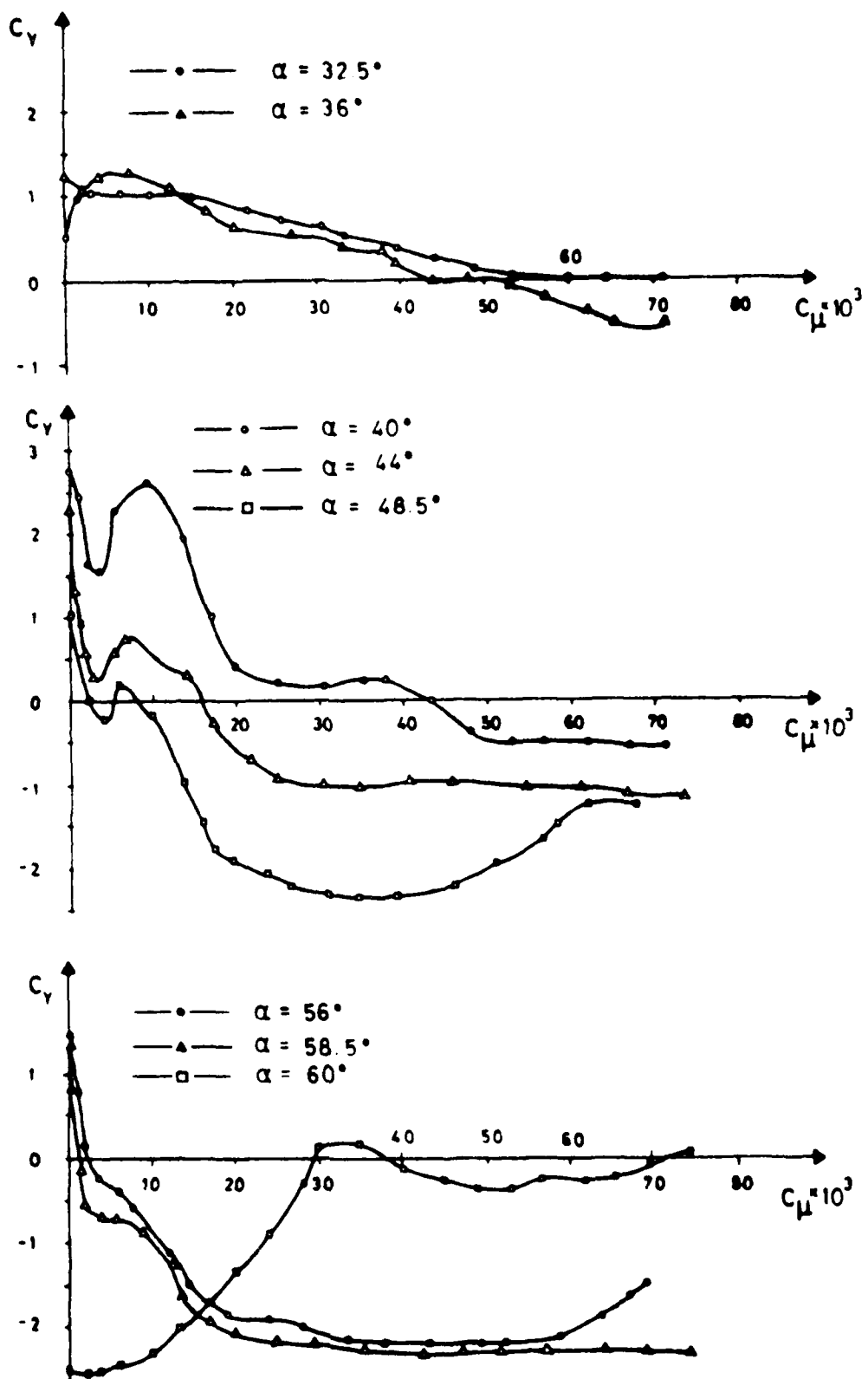
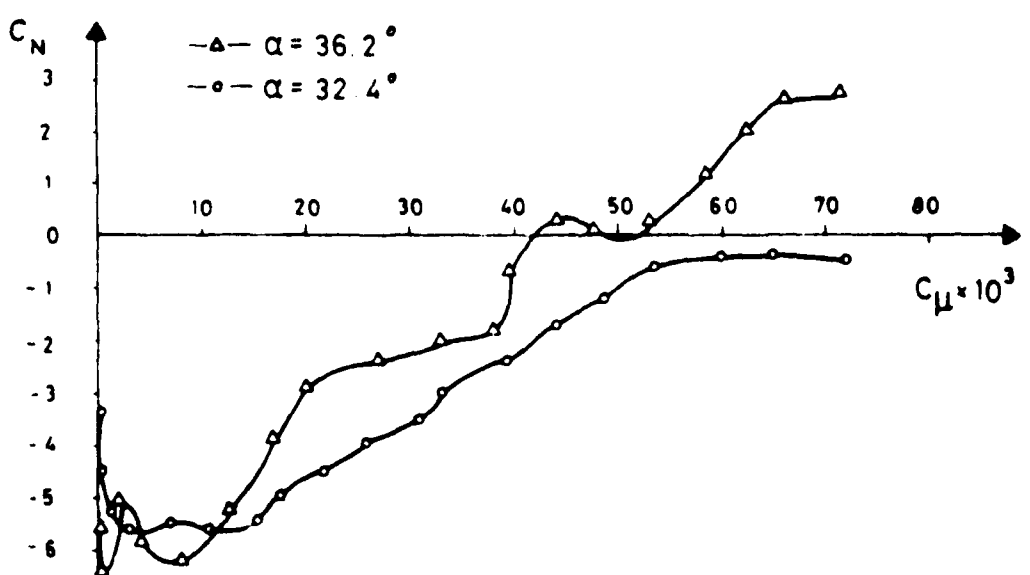
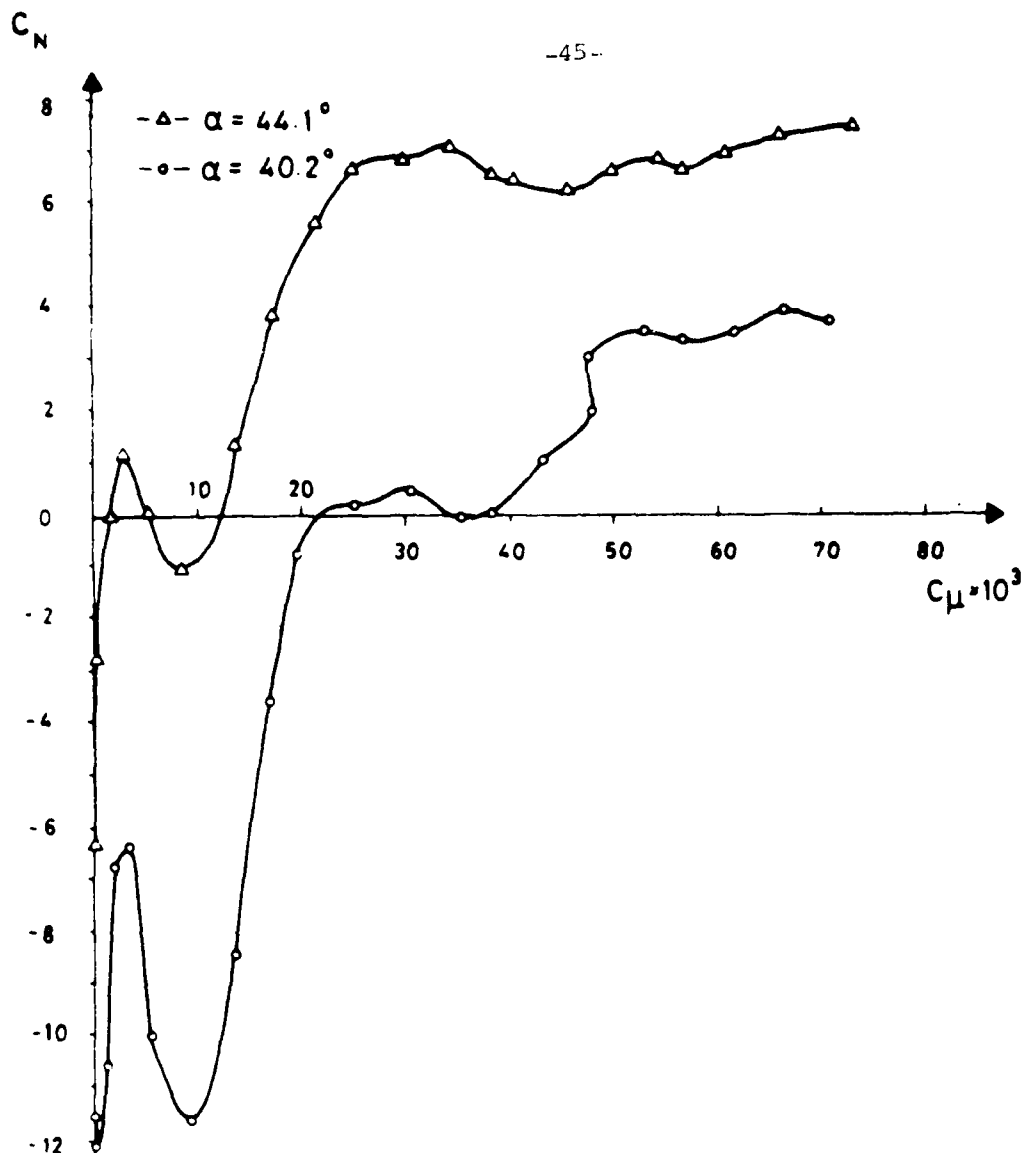


FIGURE No. 7 - VARIATION OF SIDE FORCE COEFFICIENT VS. BLOWING RATE COEFFICIENT, AT VARIOUS ANGLES OF ATTACK, $V = 32$ m/sec, WITH TRANSITION STRIP at $\pi/d = 0.333$.



VARIATION OF YAWING MOMENT COEFFICIENT Vs. BLOWING RATE
 FIGURE No. 8 - COEFFICIENT, AT VARIOUS ANGLES OF ATTACK, $V = 32$ m/sec,
 WITH TRANSITION STRIP AT $x/d = 0.333$.

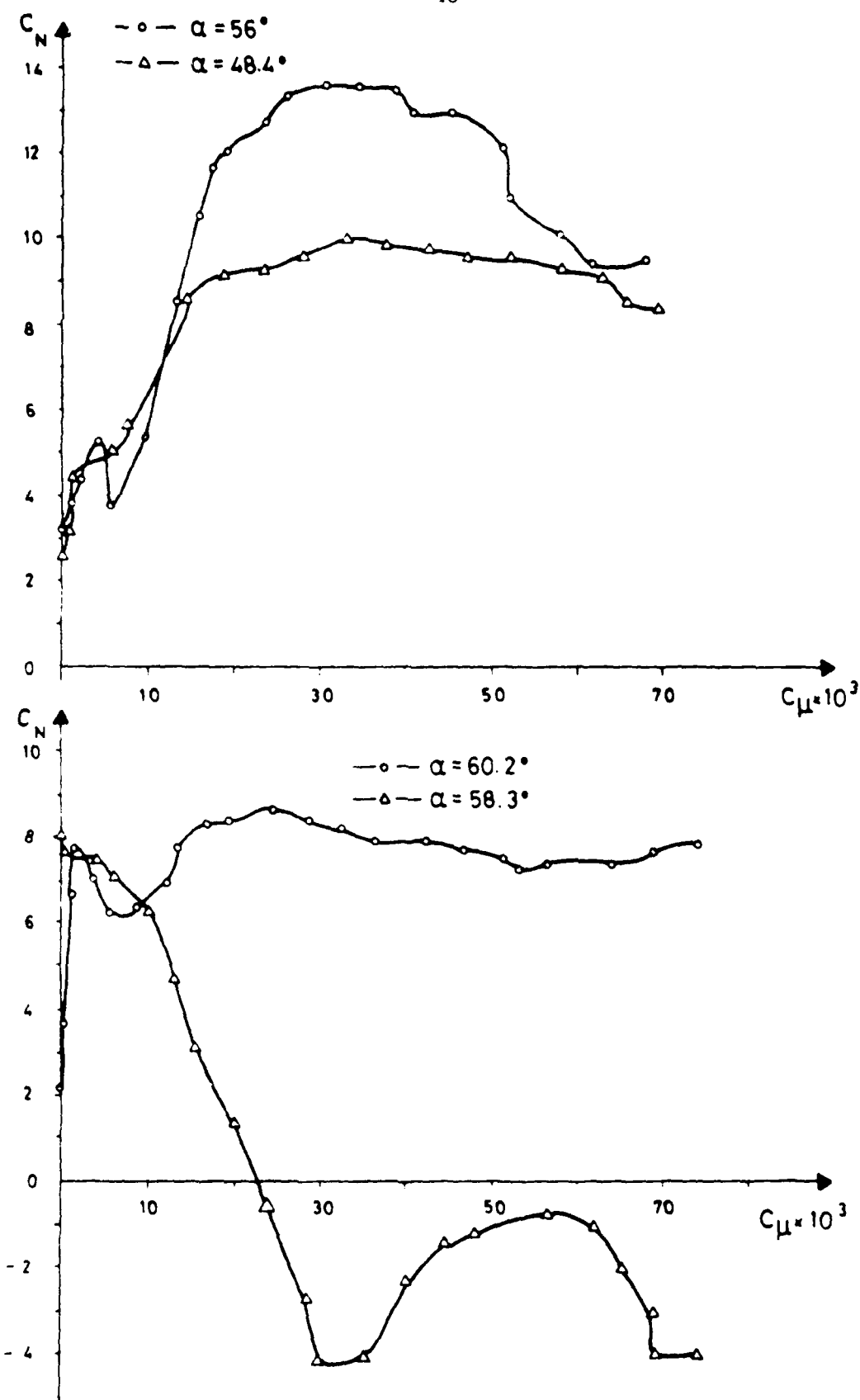


FIGURE No. 8 - CONTINUED

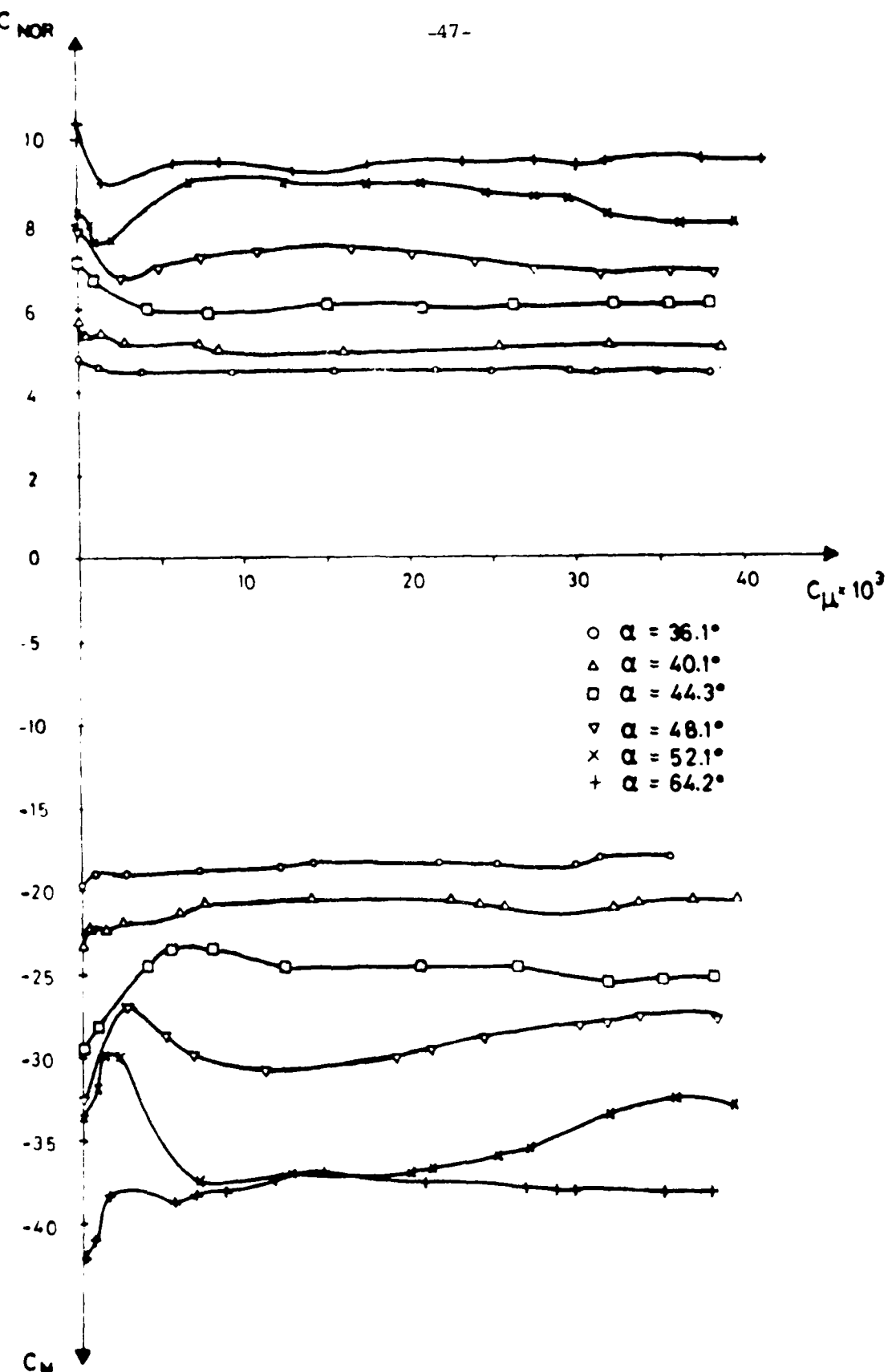


FIGURE No. 9 - NORMAL FORCE COEFFICIENT AND PITCHING MOMENT COEFFICIENT
VS. BLOWING RATE COEFFICIENT, AT VARIOUS ANGLES OF ATTACK,
 $V = 32 \text{ m/sec}$, NO TRANSITION STRIP.

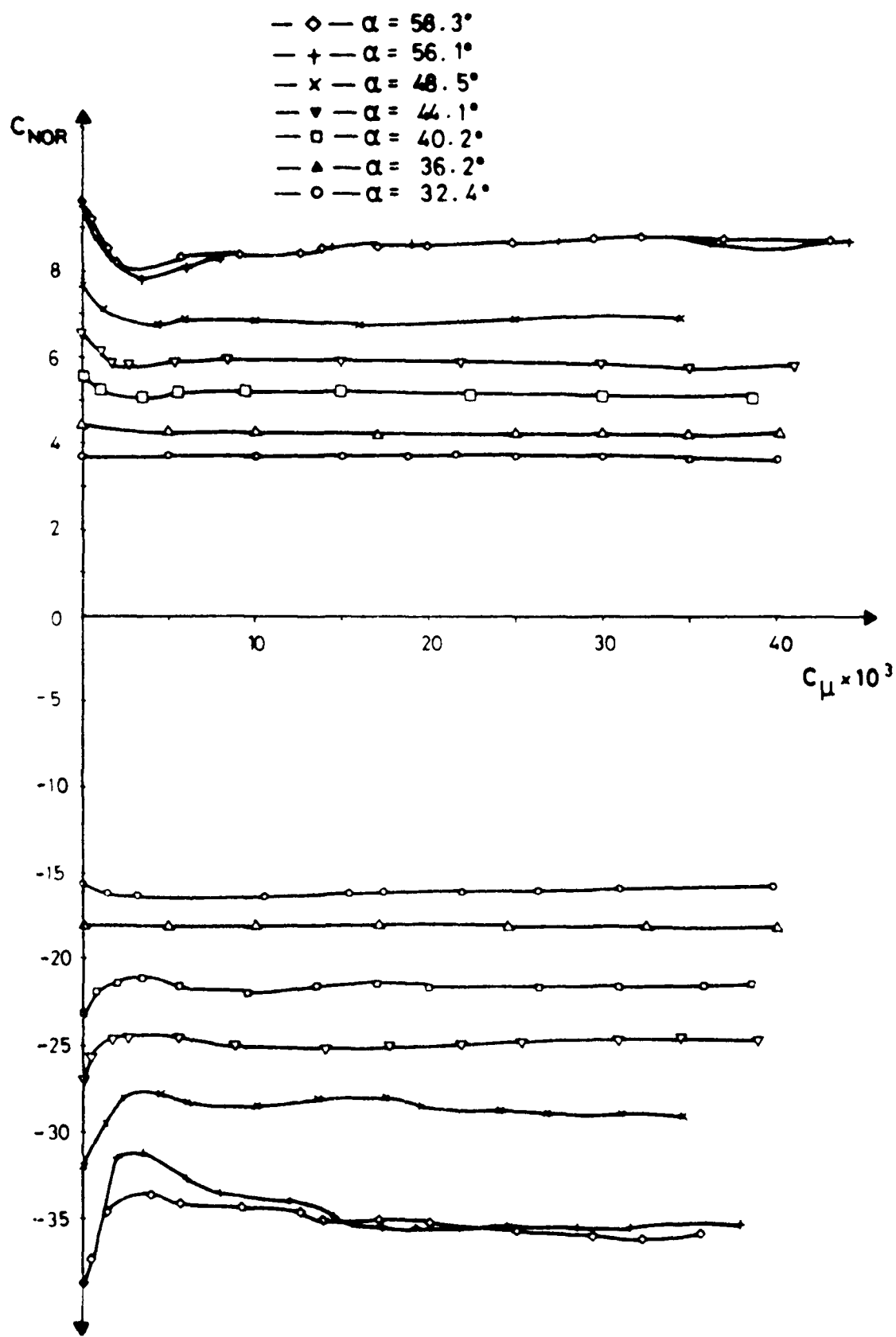


FIGURE No. 10 - NORMAL FORCE COEFFICIENT AND PITCHING MOMENT COEFFICIENT
VS. BLOWING RATE COEFFICIENT, AT VARIOUS ANGLES OF ATTACK,
 $V = 32 \text{ m/sec}$, WITH TRANSITION STRIP AT $x/d = 0.333$.

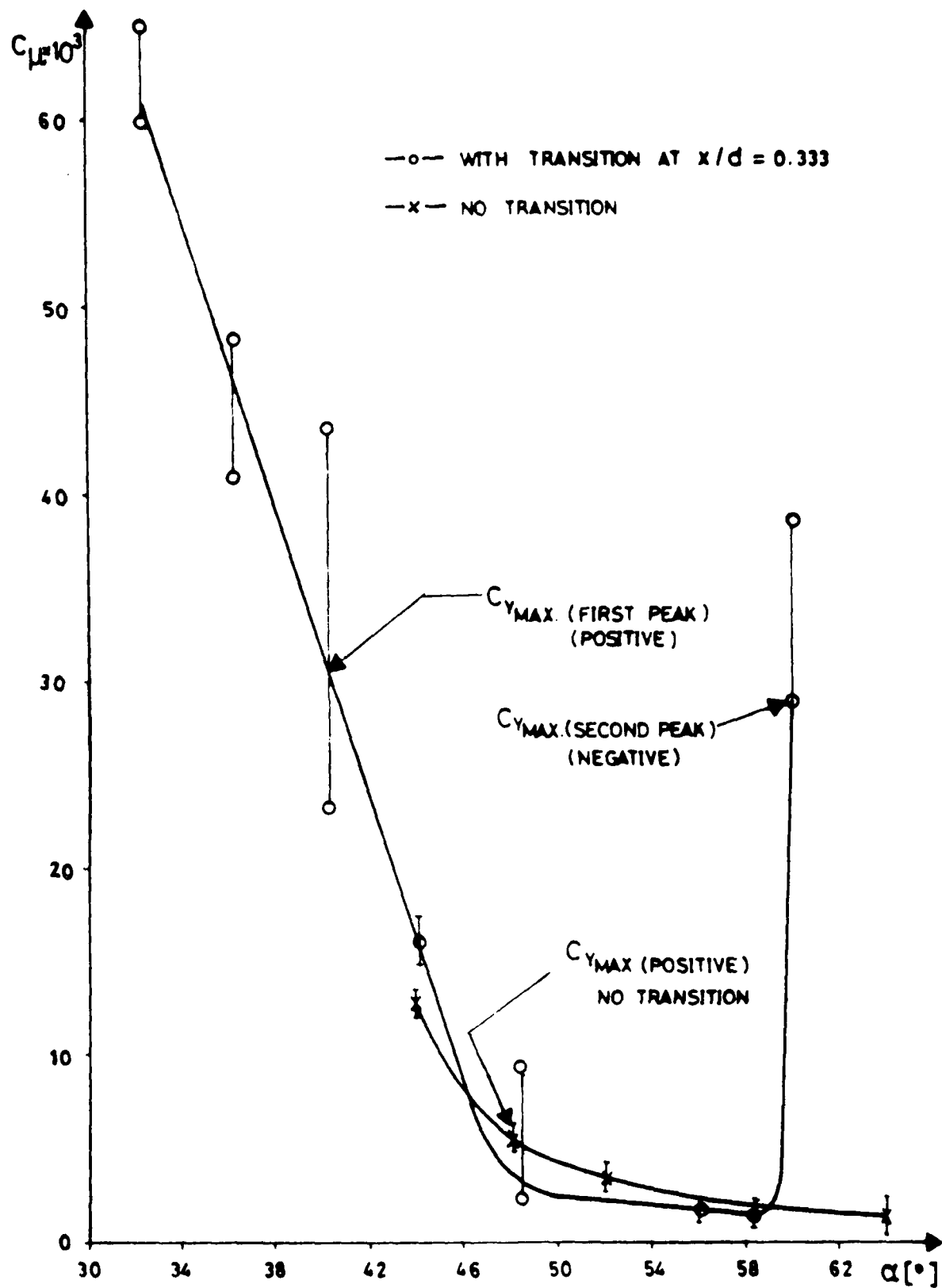


FIGURE No. 11 - BLOWING RATE COEFFICIENT NEEDED FOR SIDE FORCE ALLEVIATION AT VARIOUS ANGLES OF ATTACK.

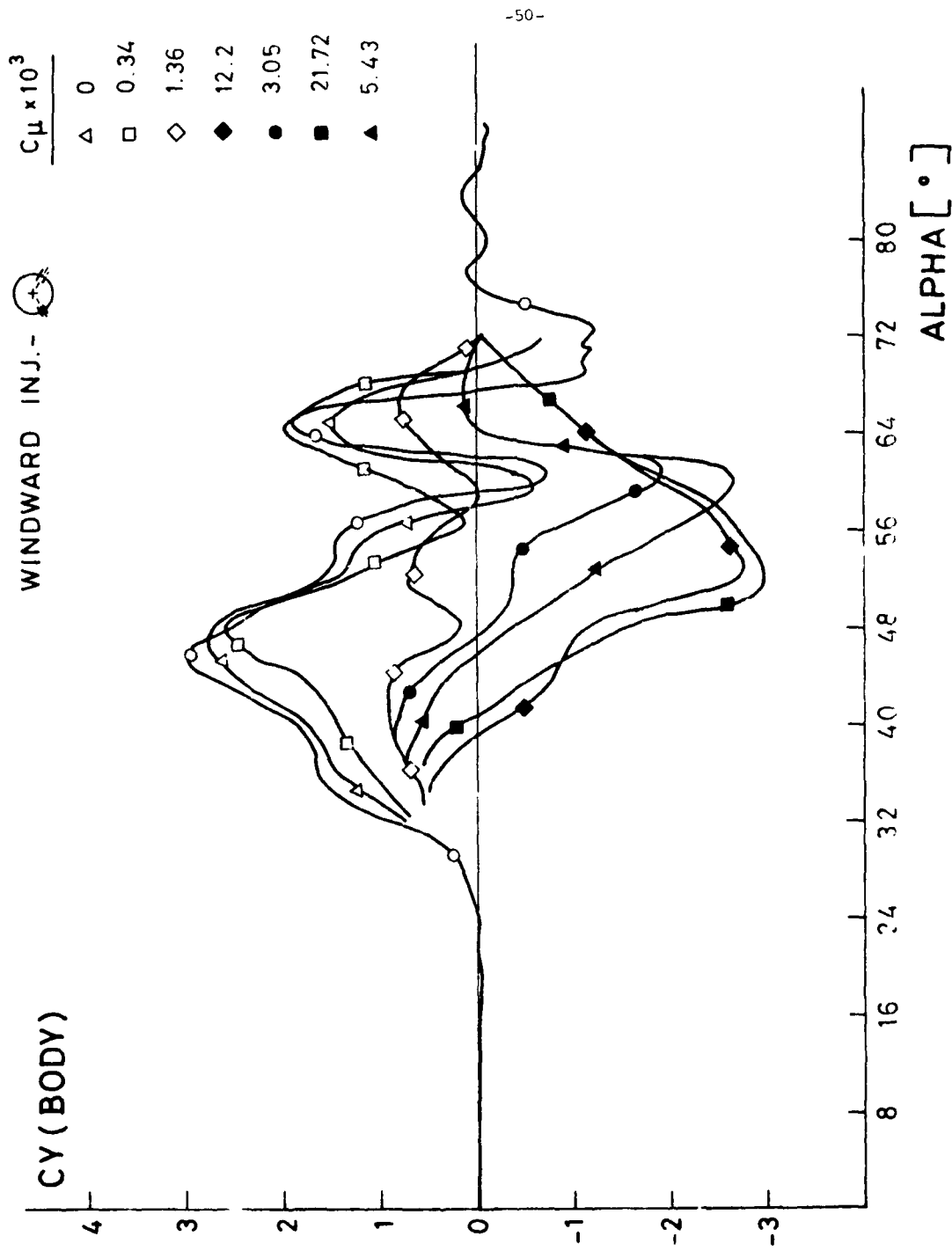


FIGURE NO. 12 - VARIATION OF SIDE FORCE COEFFICIENT VS. ANGLE OF ATTACK FOR DIFFERENT AMOUNTS OF BLOWING RATE COEFFICIENT, FOR WINDWARD AND LEEWARD JET BLOWING.

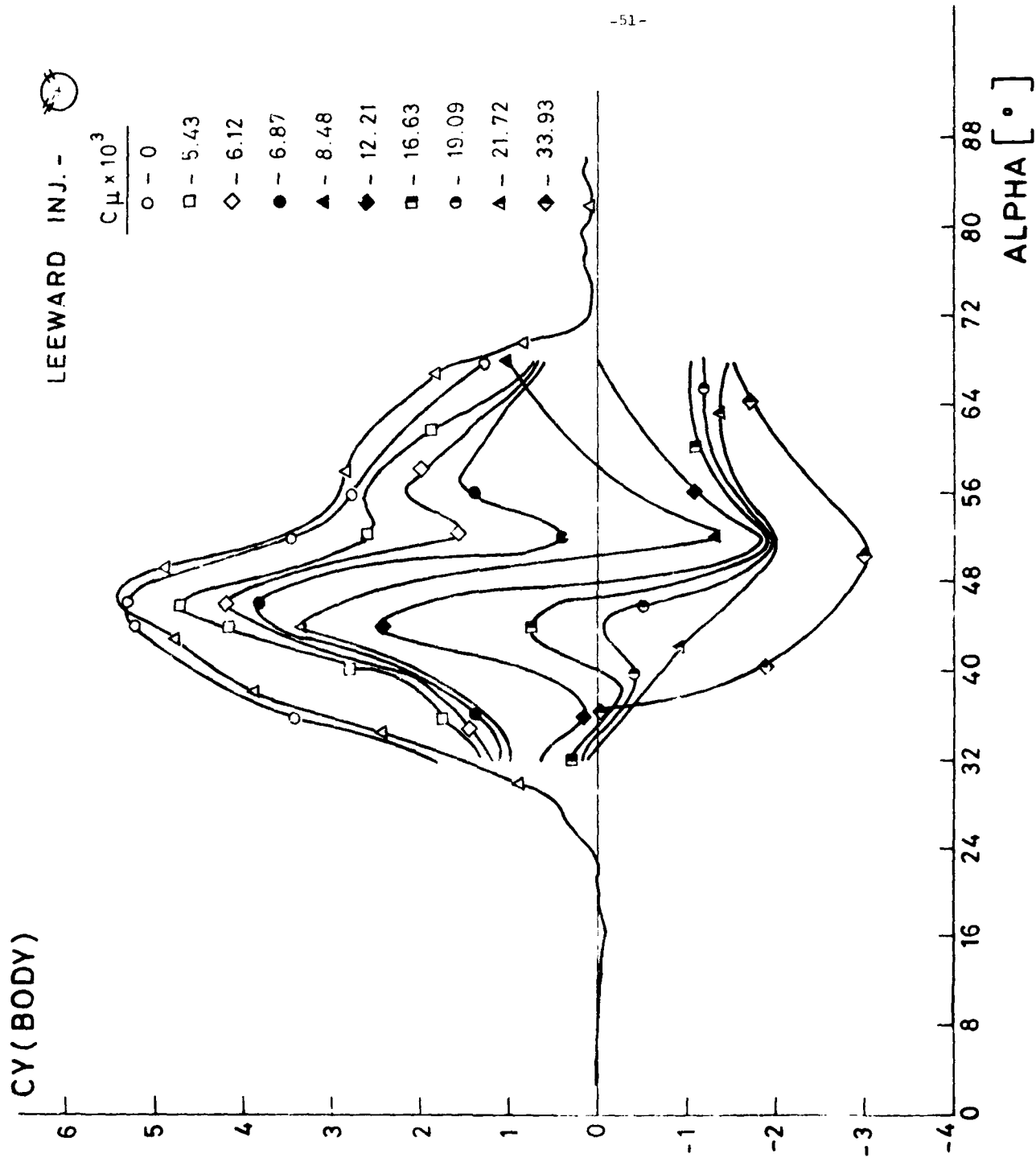


FIGURE NO. 12 - CONTINUED

○ LEEWARD INJ. 

△ { WINDWARD INJ. 

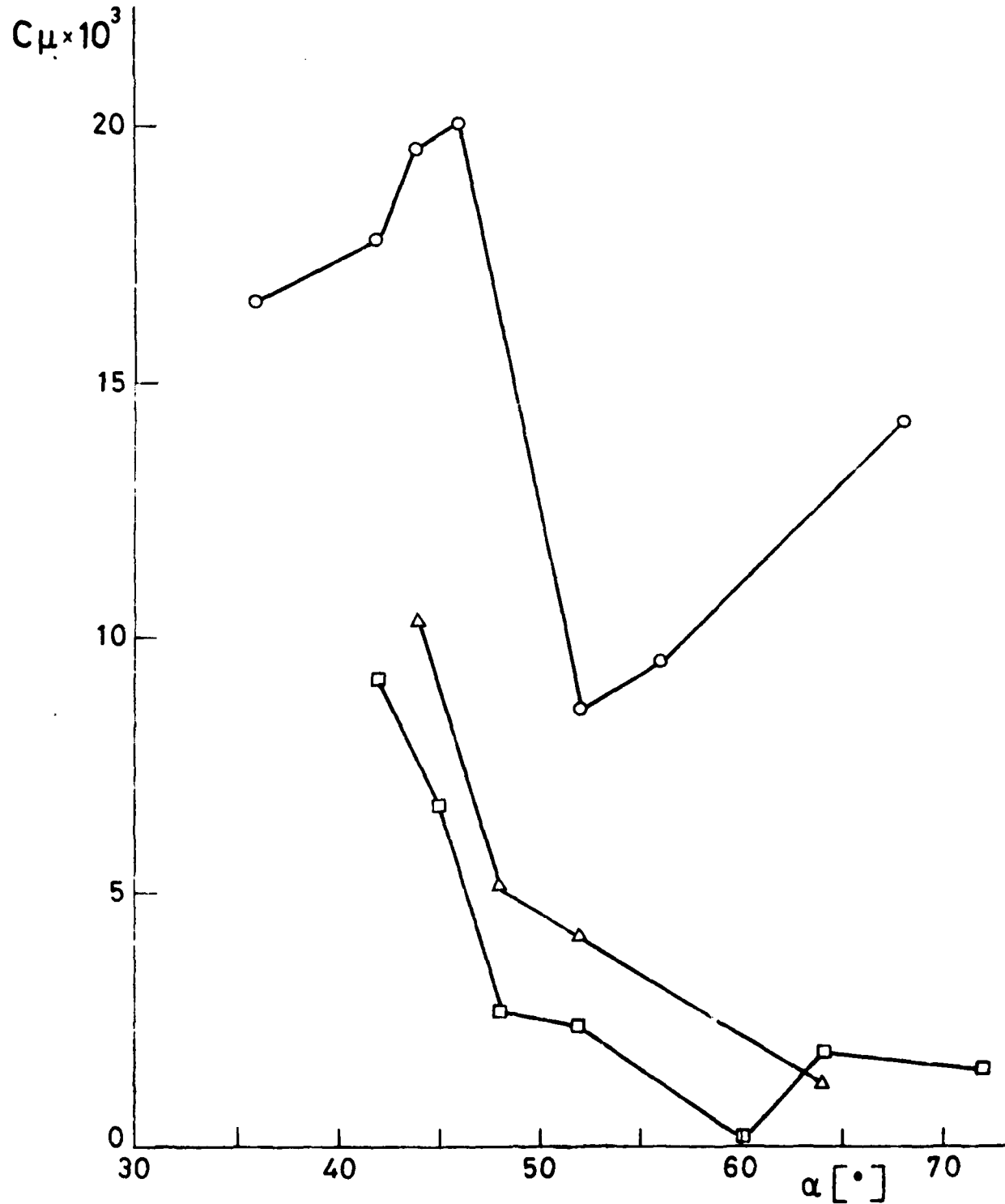


FIGURE No. 13 - AMOUNT OF BLOWING RATE COEFFICIENT NEEDED FOR SIDE FORCE ALLEVIATION AT VARIOUS ANGLES OF ATTACK.

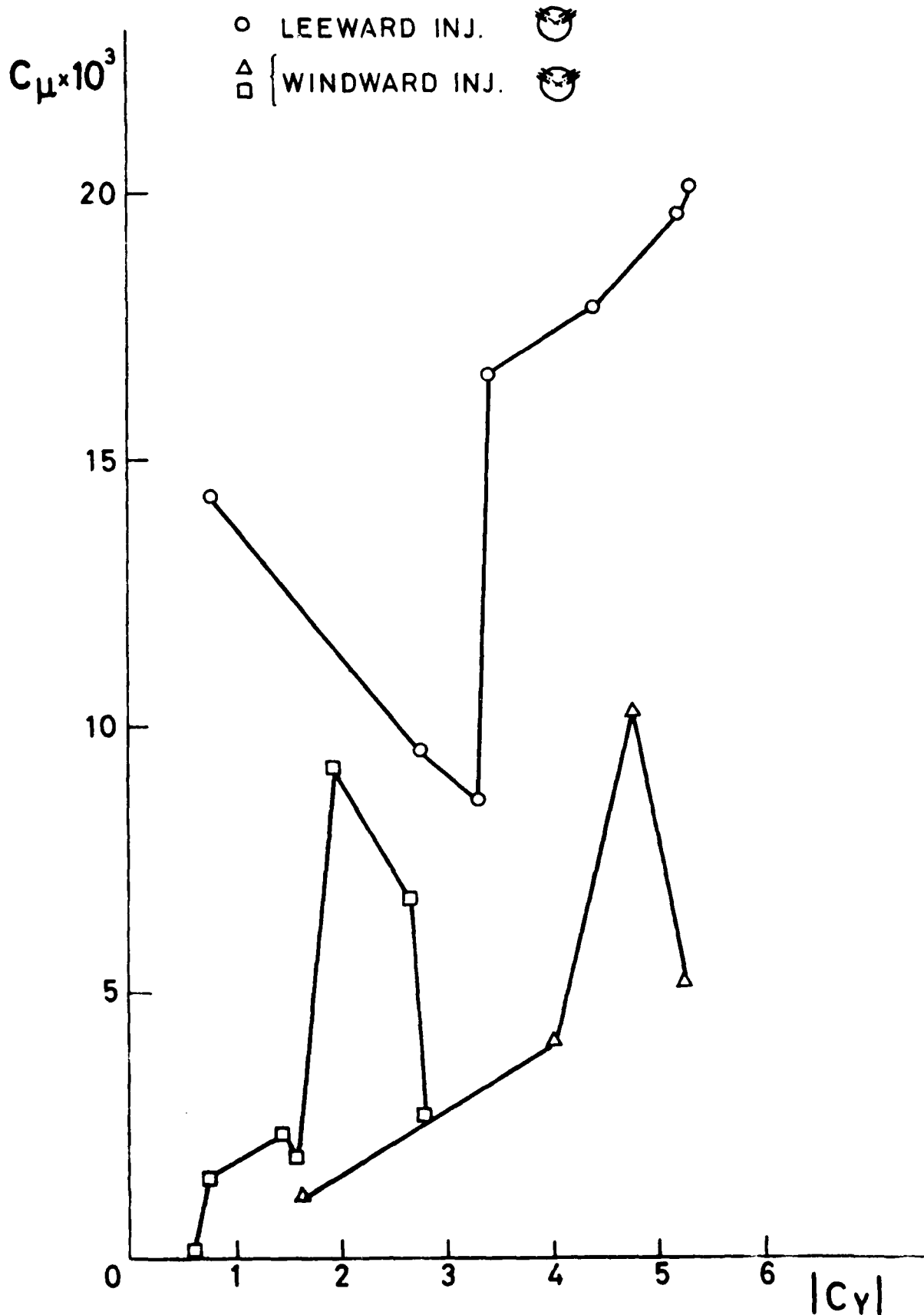


FIGURE NO. 14 - AMOUNT OF BLOWING RATE COEFFICIENT NEEDED FOR SIDE FORCE ALLEVIATION FOR VARIOUS AMOUNTS OF SIDEFORCE.

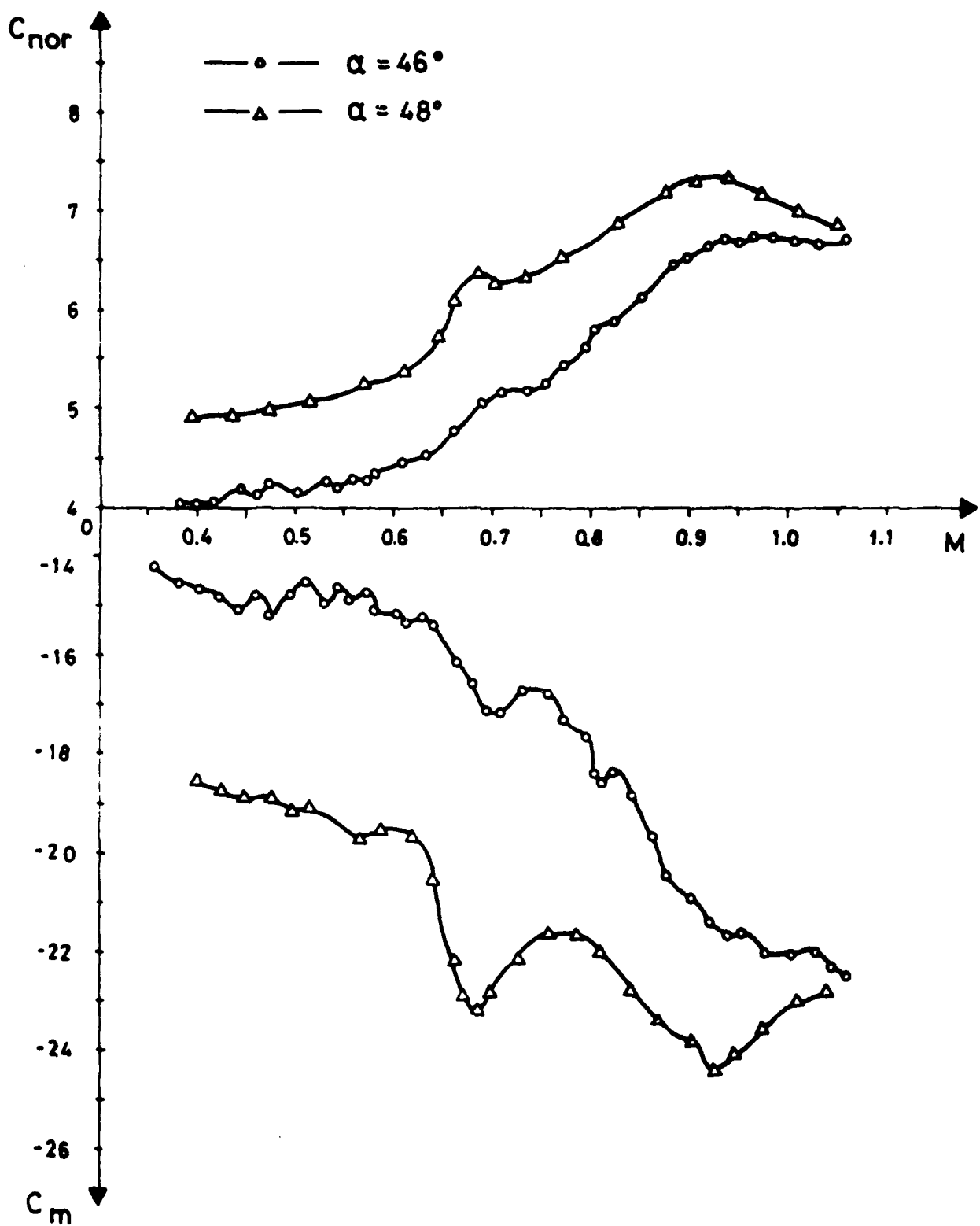


FIGURE No. 15 - NORMAL FORCE AND PITCHING MOMENT COEFFICIENTS Vs MACH NUMBER, AT TWO ANGLES OF ATTACK, NO TRANSITION STRIP, NO INJECTION.

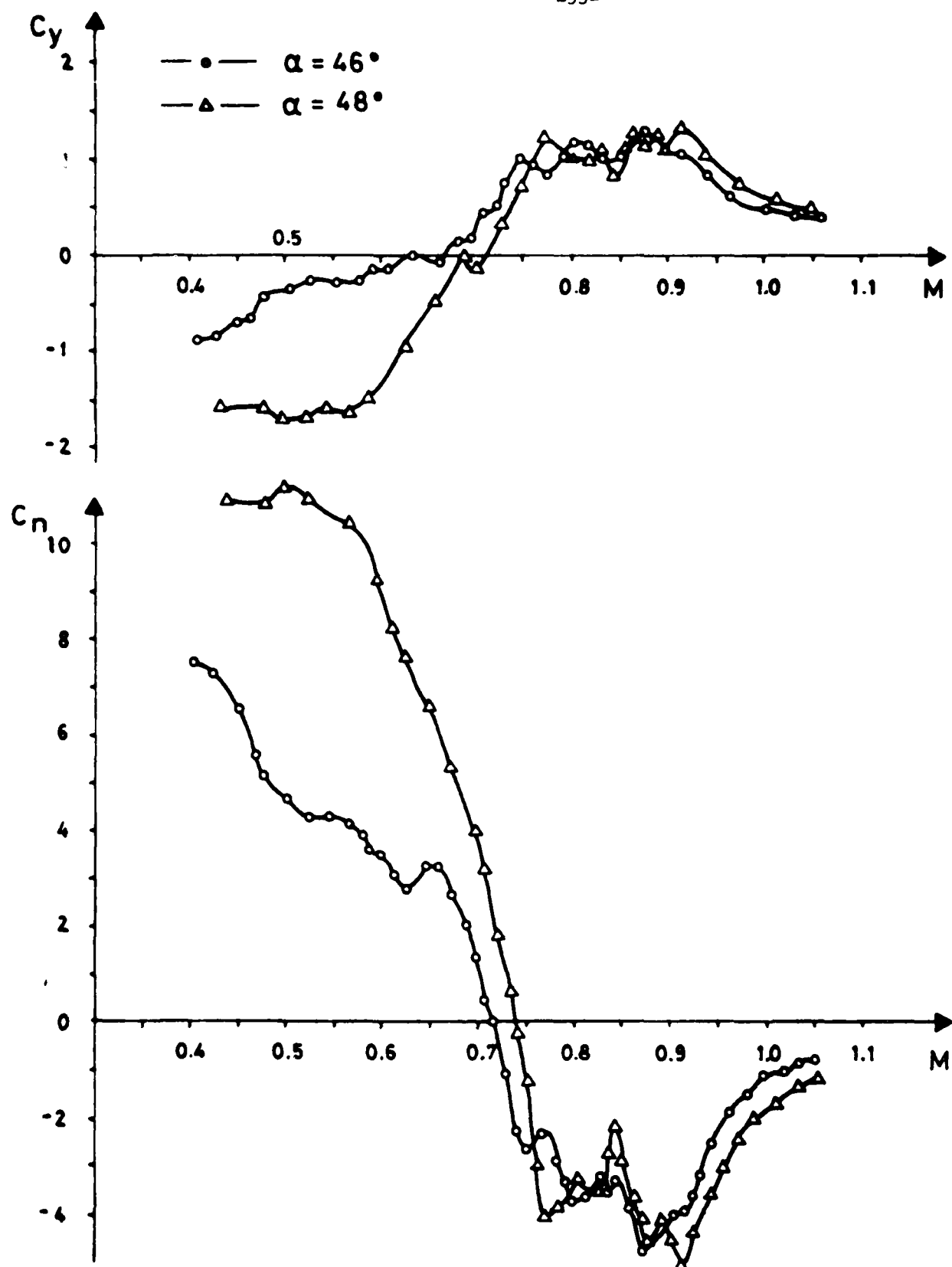


FIGURE No. 16 - SIDE FORCE AND YAWING MOMENT COEFFICIENT VS. MACH NUMBER,
AT TWO ANGLES OF ATTACK, NO TRANSITION STRIP, NO INJECTION.

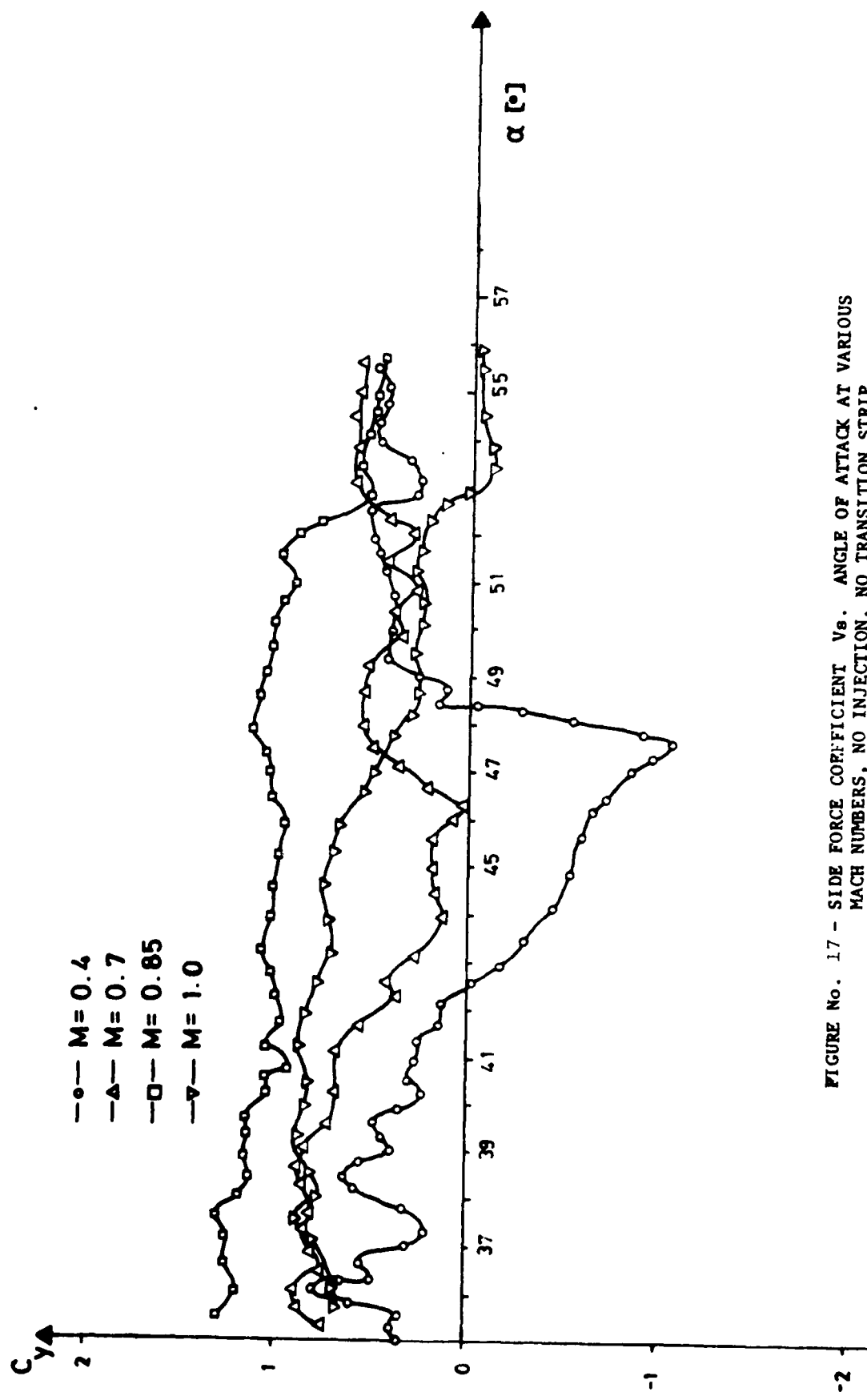


FIGURE NO. 17 - SIDE FORCE COEFFICIENT VS. ANGLE OF ATTACK AT VARIOUS MACH NUMBERS, NO INJECTION, NO TRANSITION STRIP.

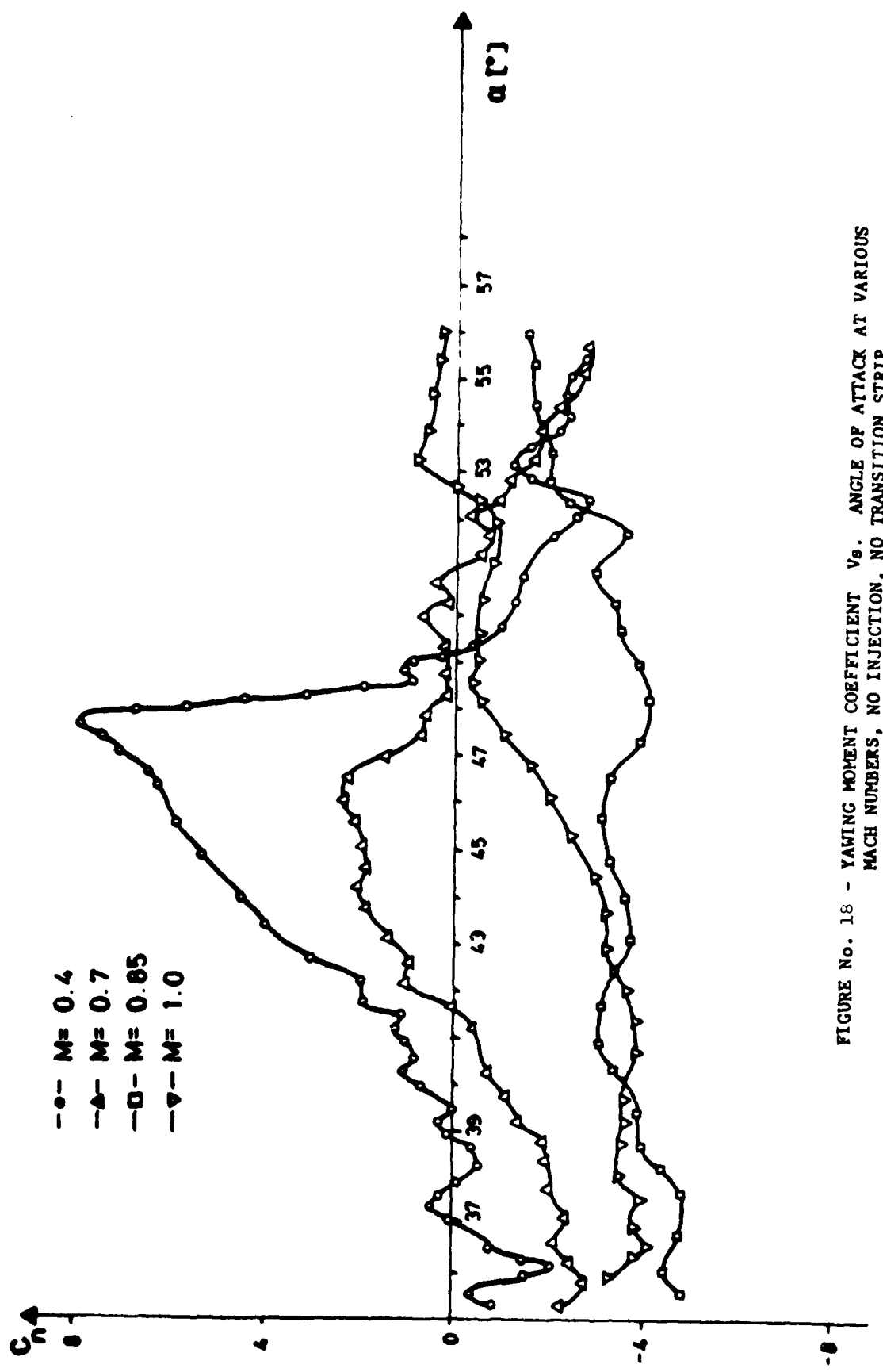


FIGURE NO. 18 - YAWING MOMENT COEFFICIENT C_n VS. ANGLE OF ATTACK AT VARIOUS MACH NUMBERS, NO INJECTION, NO TRANSITION STRIP.

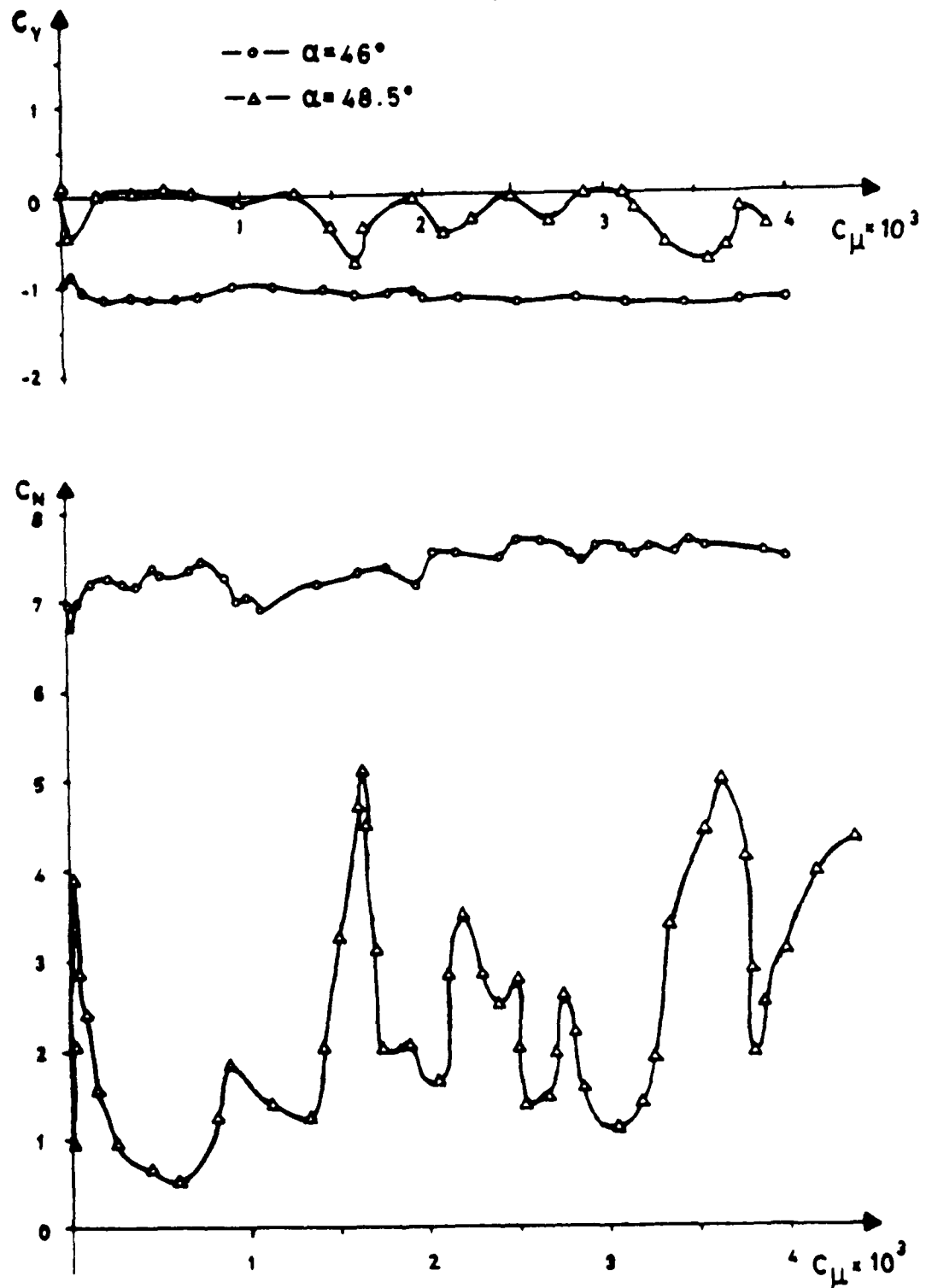


FIGURE No. 19 - SIDE FORCE AND YAWING MOMENT COEFFICIENTS VS. BLOWING RATE COEFFICIENT AT $M = 0.4$, AT TWO ANGLES OF ATTACK, NO TRANSITION STRIP.

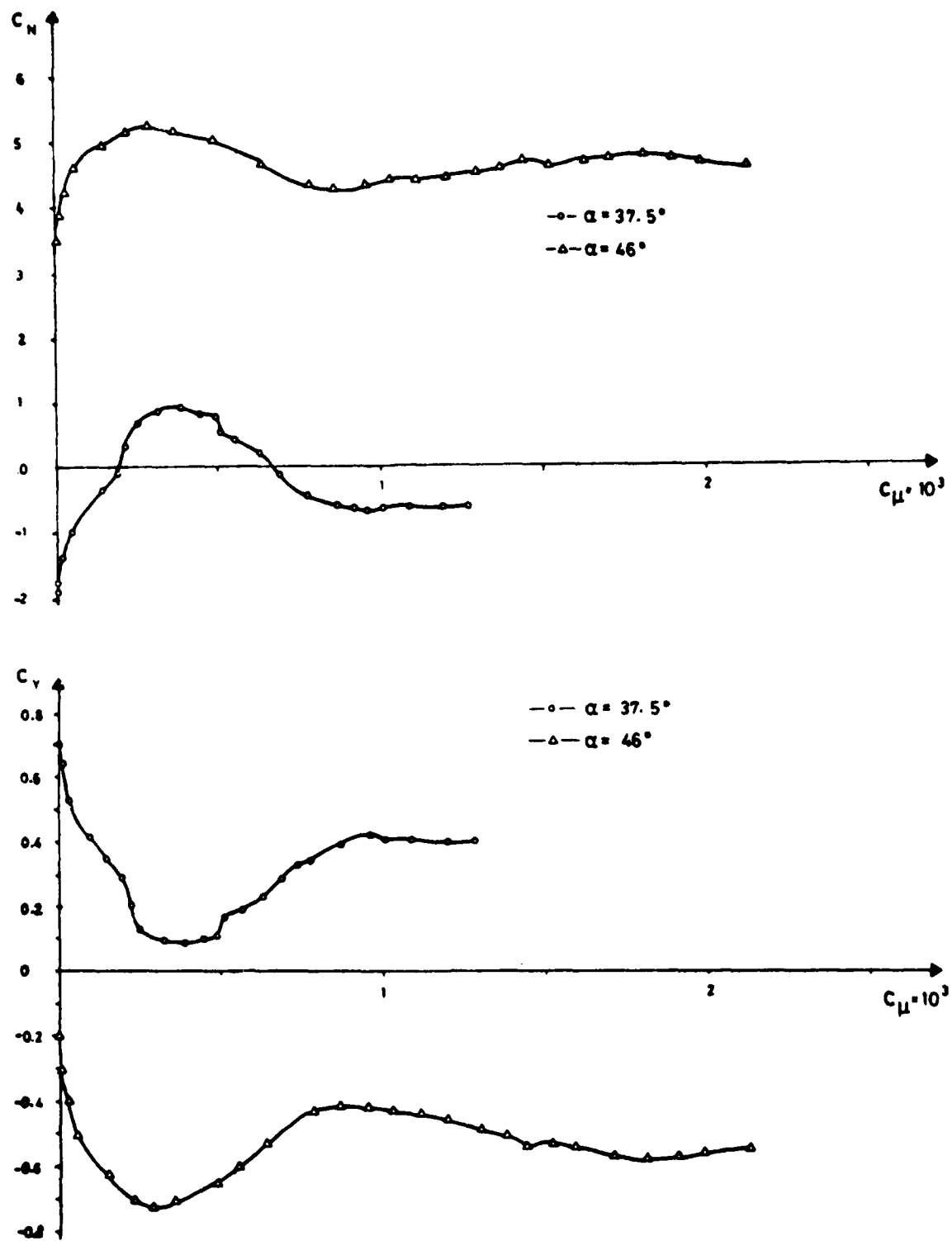


FIGURE No. 20 - SIDE FORCE AND YAWING MOMENT COEFFICIENTS Vs. BLOWING RATE COEFFICIENT AT $M = 0.7$, AT TWO ANGLES OF ATTACK.

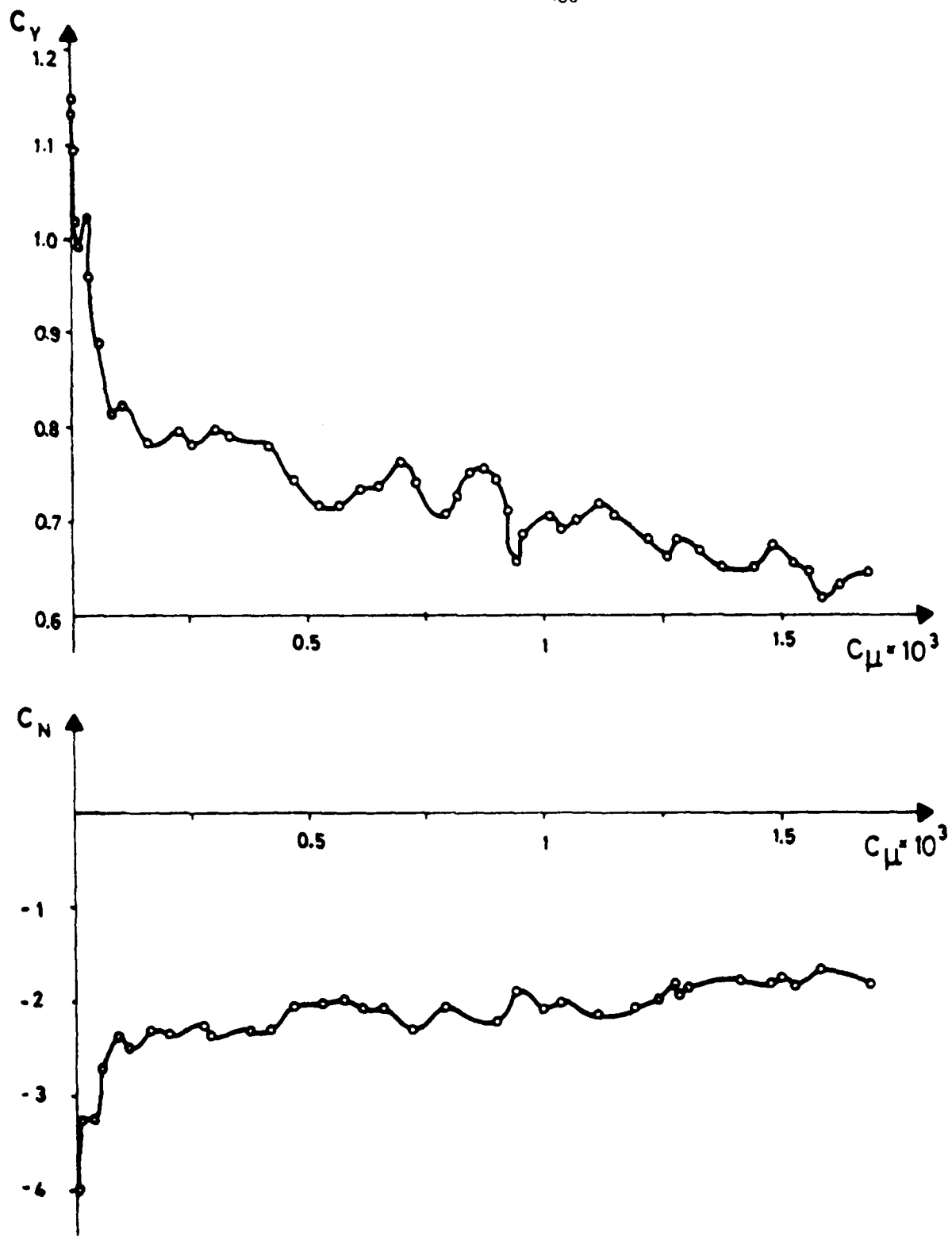


FIGURE No. 21 - SIDE FORCE AND YAWING MOMENT COEFFICIENTS VS. BLOWING RATE COEFFICIENT AT $M = 0.85$, AT 47° ANGLE OF ATTACK.

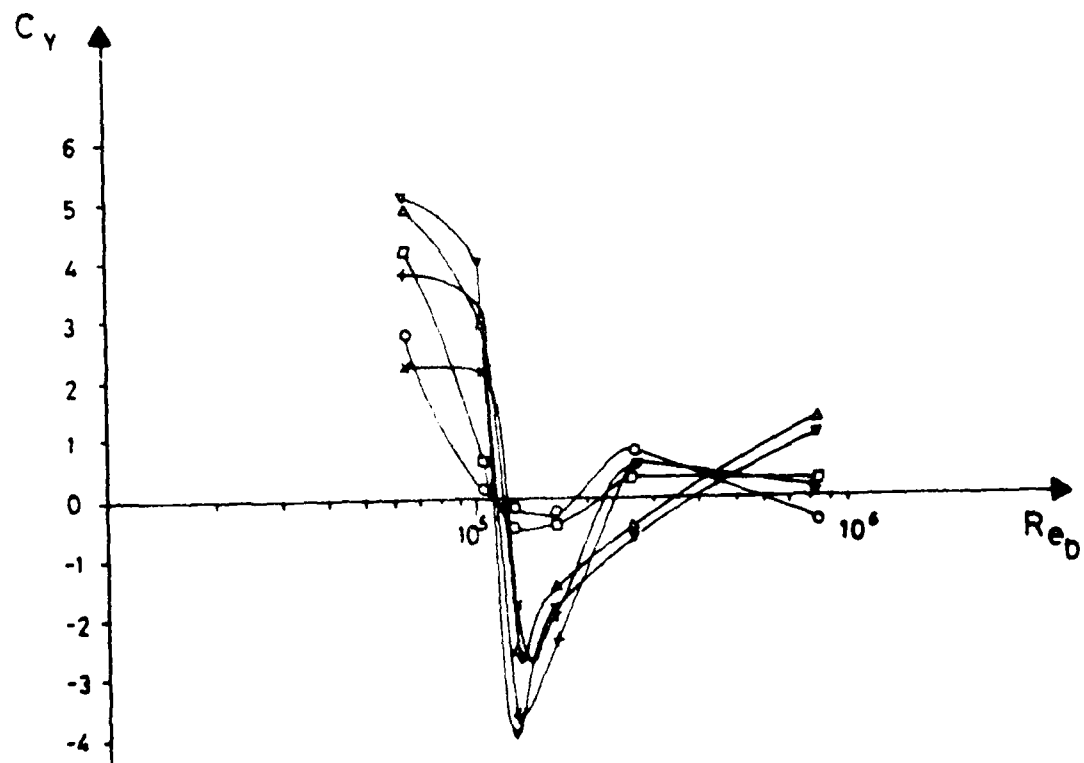
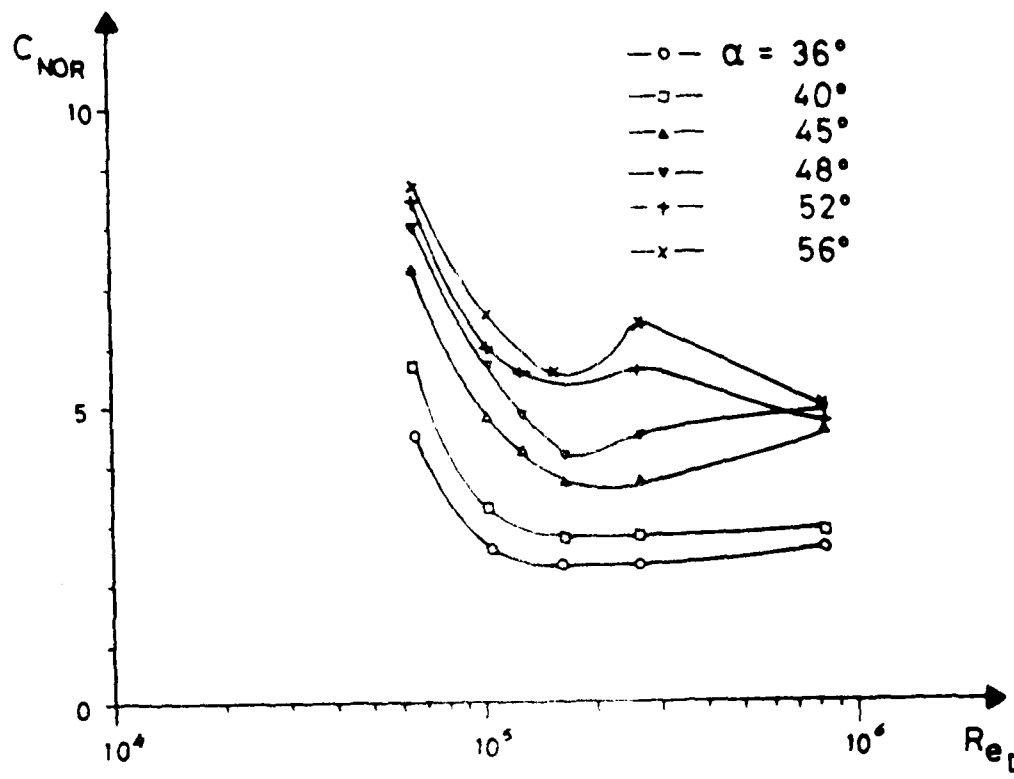


FIGURE No. 22 - NORMAL FORCE AND SIDE FORCE COEFFICIENTS Vs. REYNOLDS NUMBER, AT VARIOUS ANGLES OF ATTACK, NO TRANSITION STRIP, NO INJECTION.

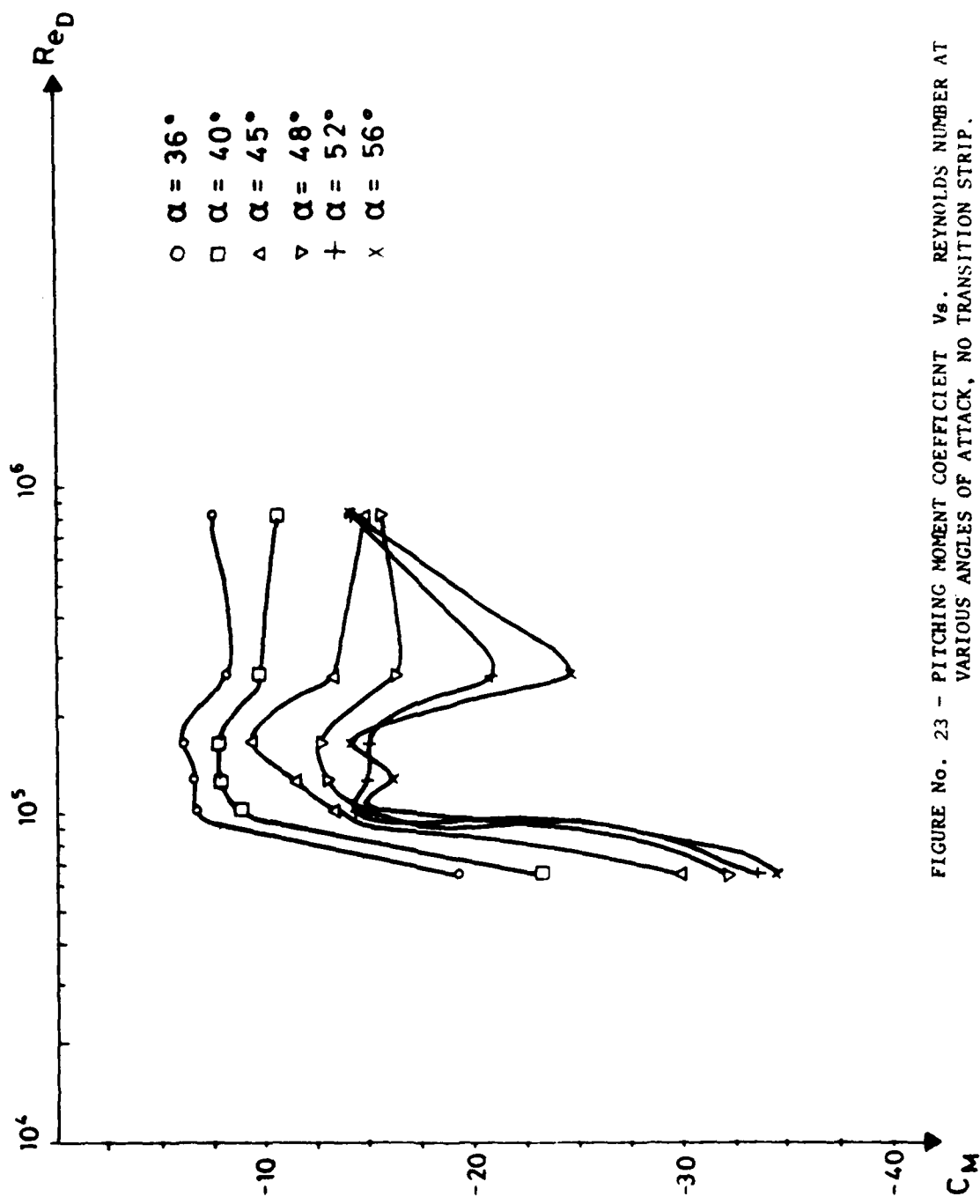


FIGURE No. 23 - PITCHING MOMENT COEFFICIENT C_M VS. REYNOLDS NUMBER AT VARIOUS ANGLES OF ATTACK, NO TRANSITION STRIP.

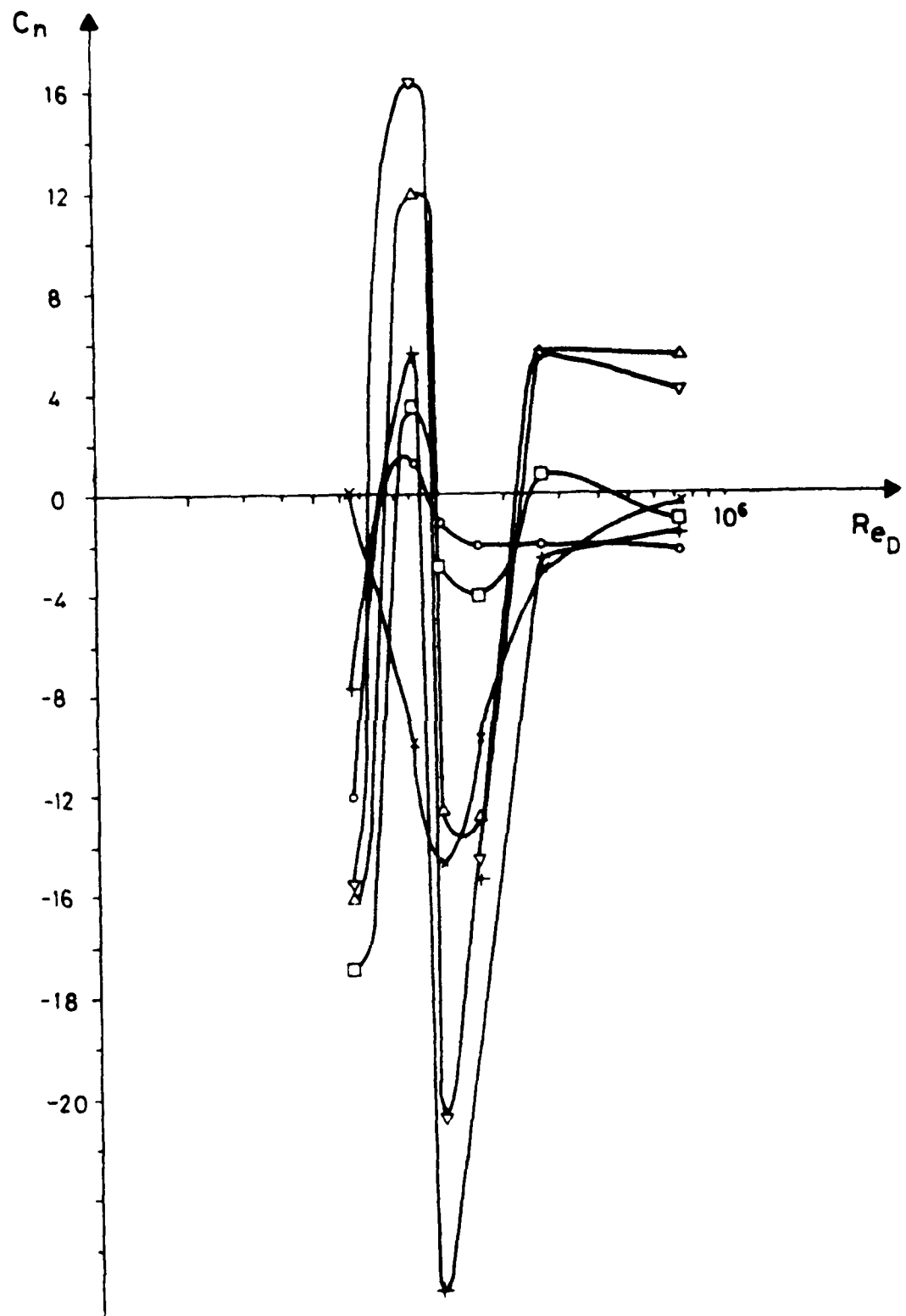
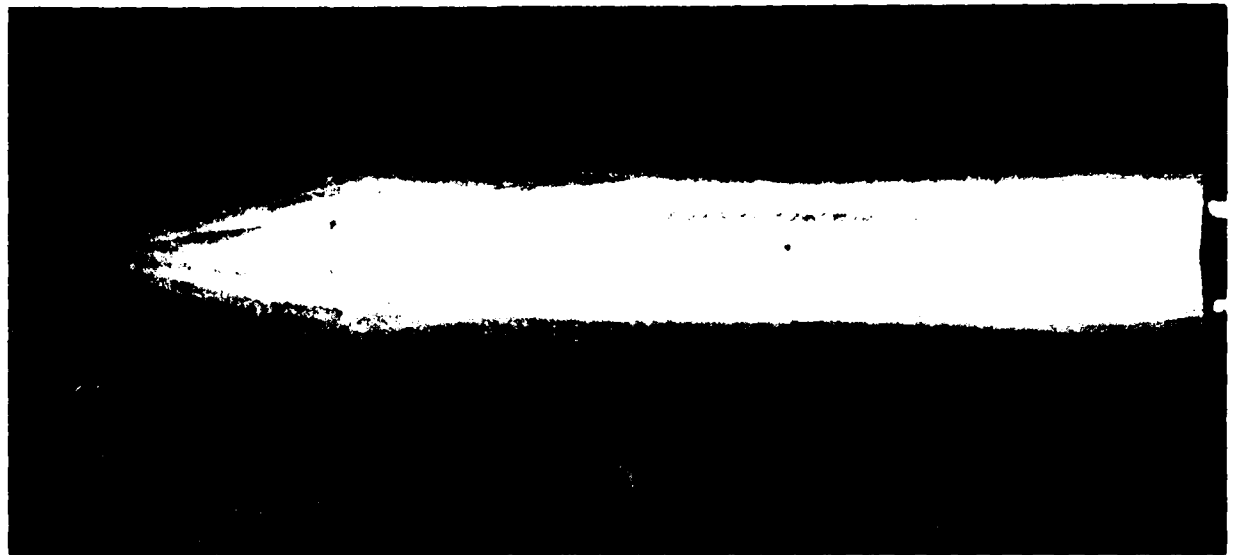
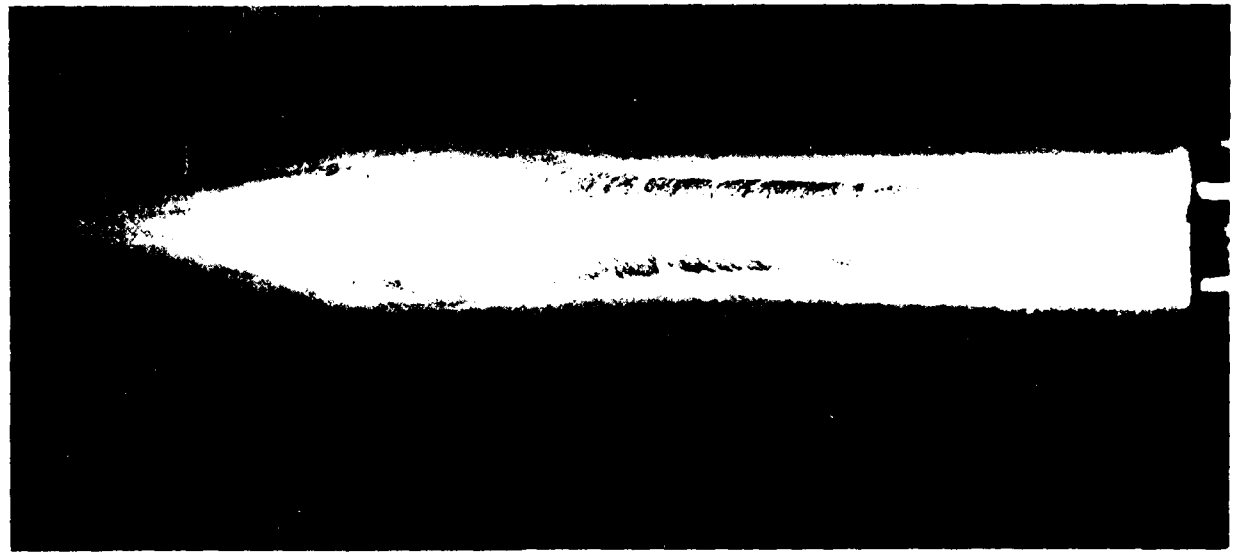


FIGURE No. 24 - YAWING MOMENT COEFFICIENT VS. REYNOLDS NUMBER, AT VARIOUS ANGLES OF ATTACK, NO TRANSITION STRIP.



NO JET BLOWING

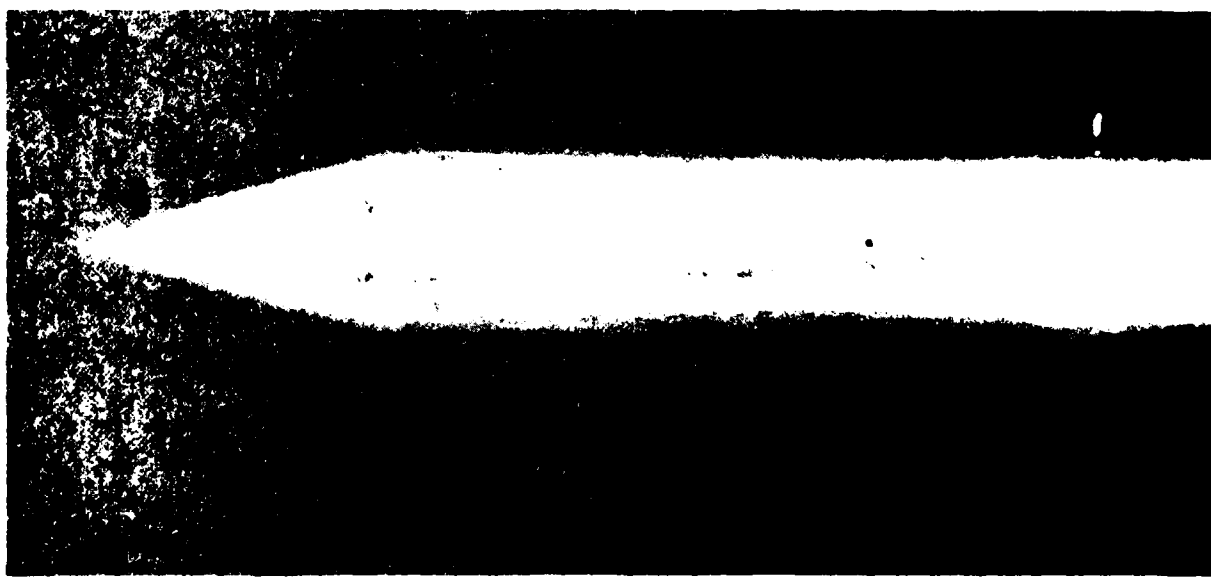


WITH JET BLOWING

FIGURE No. 25 - OIL FLOW VISUALIZATION OF THE CONE-CYLINDER MODEL AT
 $V = 32 \text{ m/sec}$, $\alpha = 40^\circ$, WITH A TRANSITION RING AT $x/D = 0.333$.

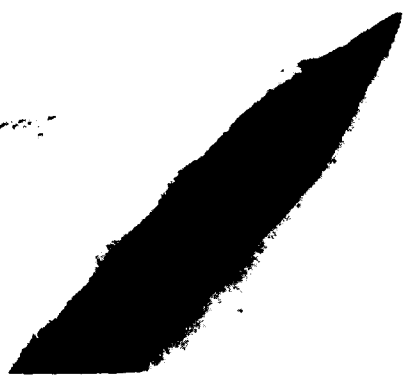


NO JET BLOWING

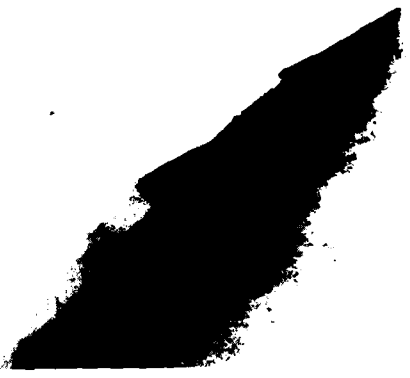


WITH JET BLOWING

FIGURE 10 - OIL FLOW VISUALIZATION OF THE CONE-CYLINDER MODEL. $U = 32$
 $m/sec.$, $\alpha = 55^\circ$, NO TRANSITION RING.



$M = 0.46$



$M = 0.71$



$M = 0.87$



$M = 1.06$

FIGURE No. 27 - SCHLIEREN PHOTOGRAPHS OF THE CONE-CYLINDER MODEL AT VARIOUS MACH NUMBERS, $\alpha = 47^\circ$, NO JET BLOWING.



Jet Blowing Off



Jet Blowing On

FIGURE No. 28 - SCHLIEREN PHOTOGRAPHS OF THE CONE CYLINDER MODEL AT $M = 0.7$,
 $\alpha = 37.5^\circ$.

PART OF A BODY, DIVIDED INTO ELEMENTAL PANELS

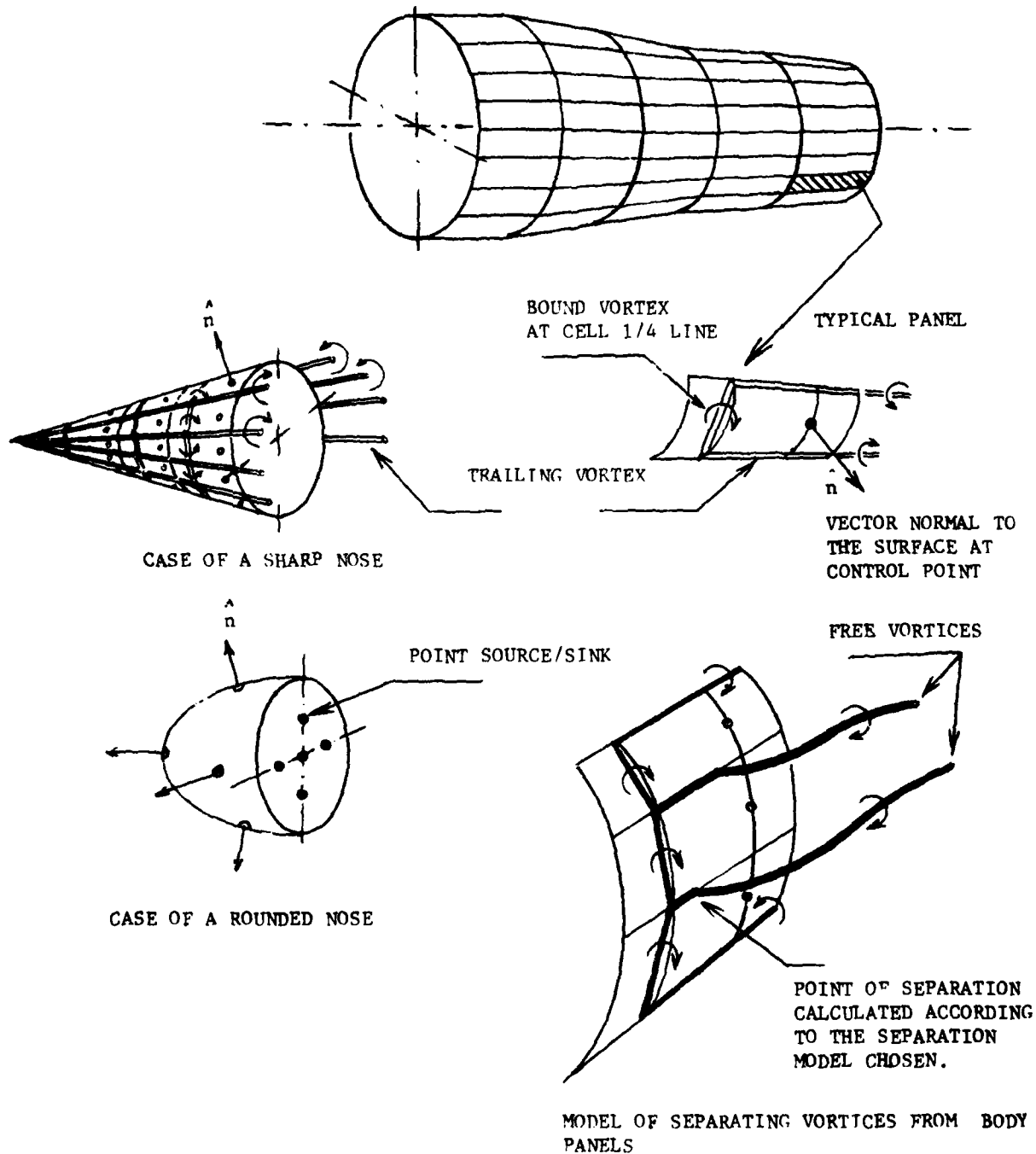


FIGURE No. 29 - ILLUSTRATION OF THE MODEL FOR BODIES INCLUDING VORTEX SEPARATION.

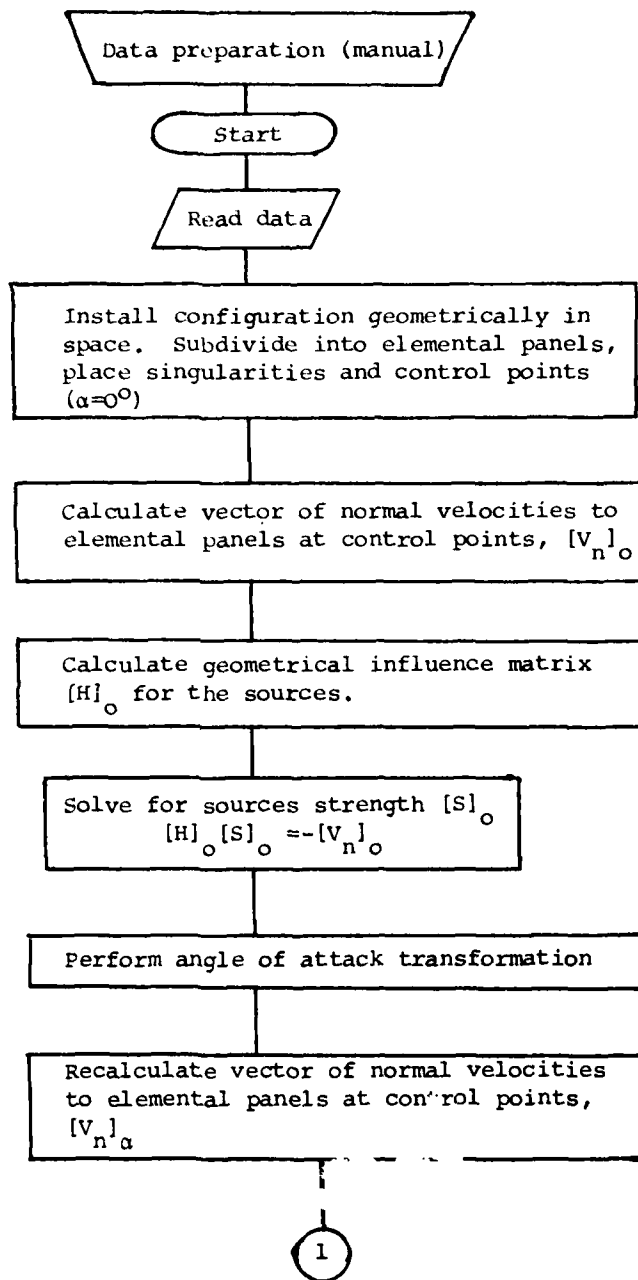


FIGURE NO. 30 - SCHEMATIC FLOW-CHART OF THE METHOD OF CALCULATION.

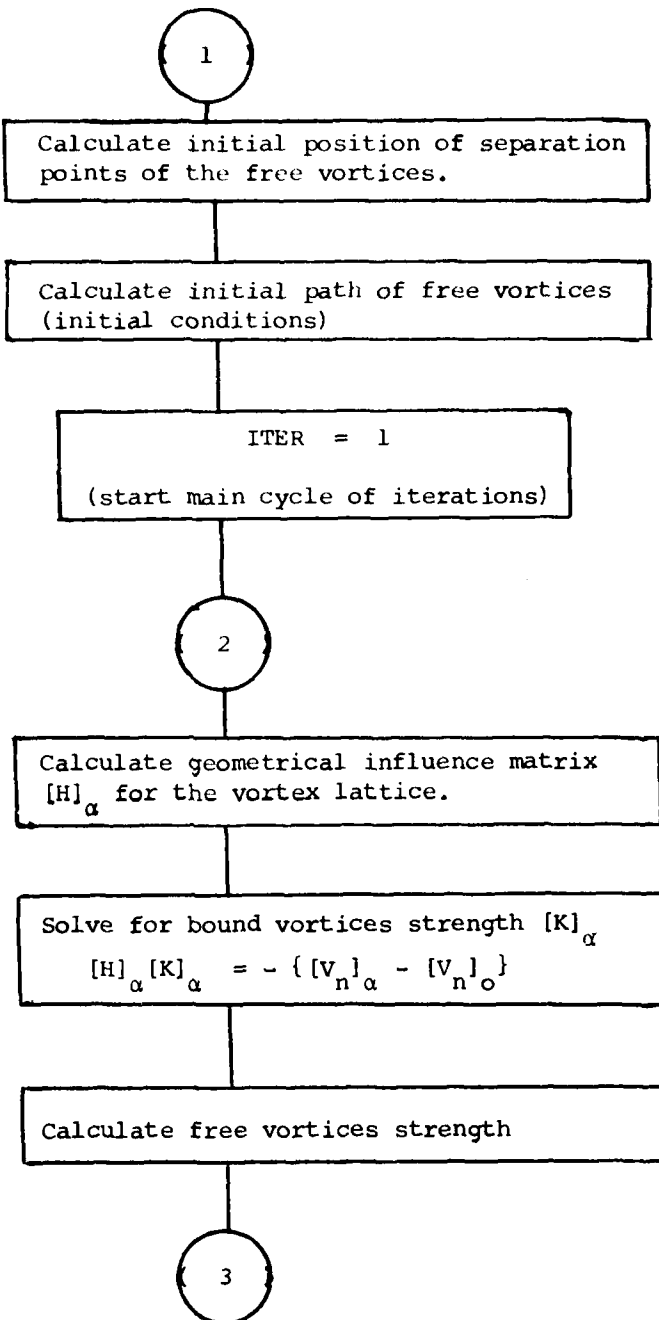


FIGURE 30 - CONTINUED.

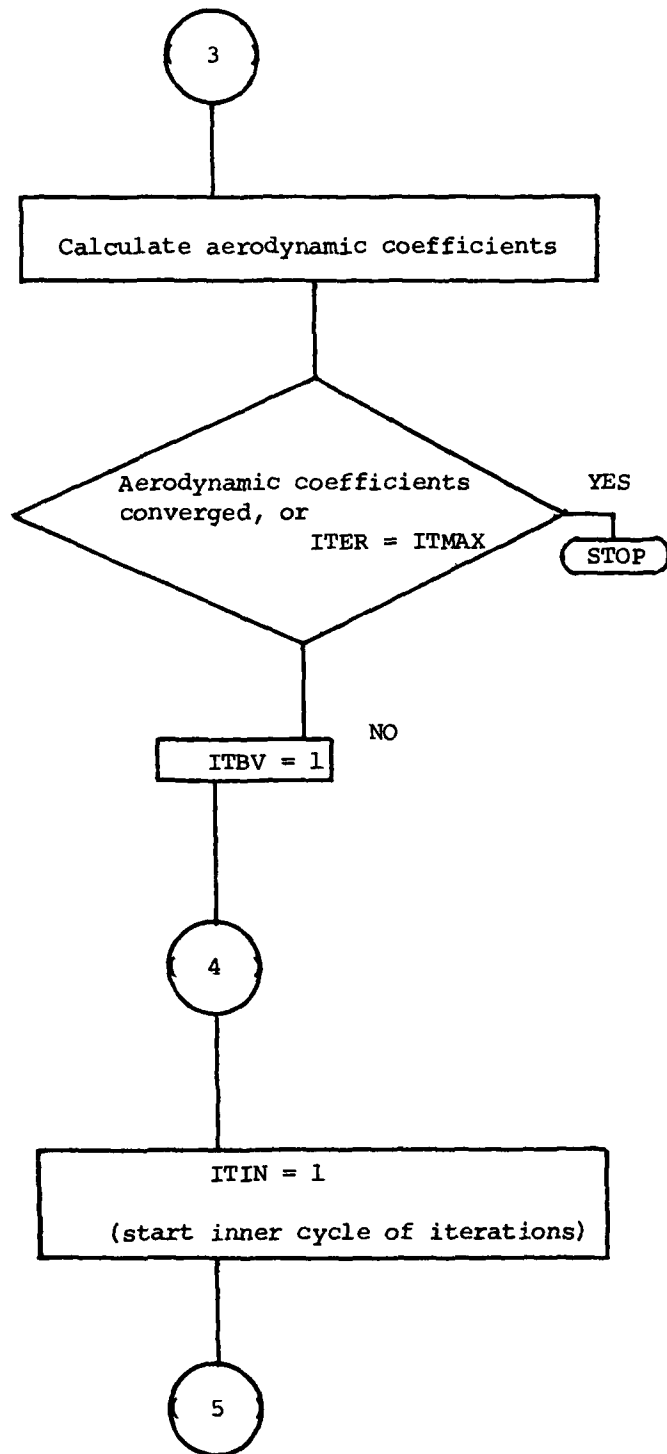


FIGURE No. 30 - CONTINUED.

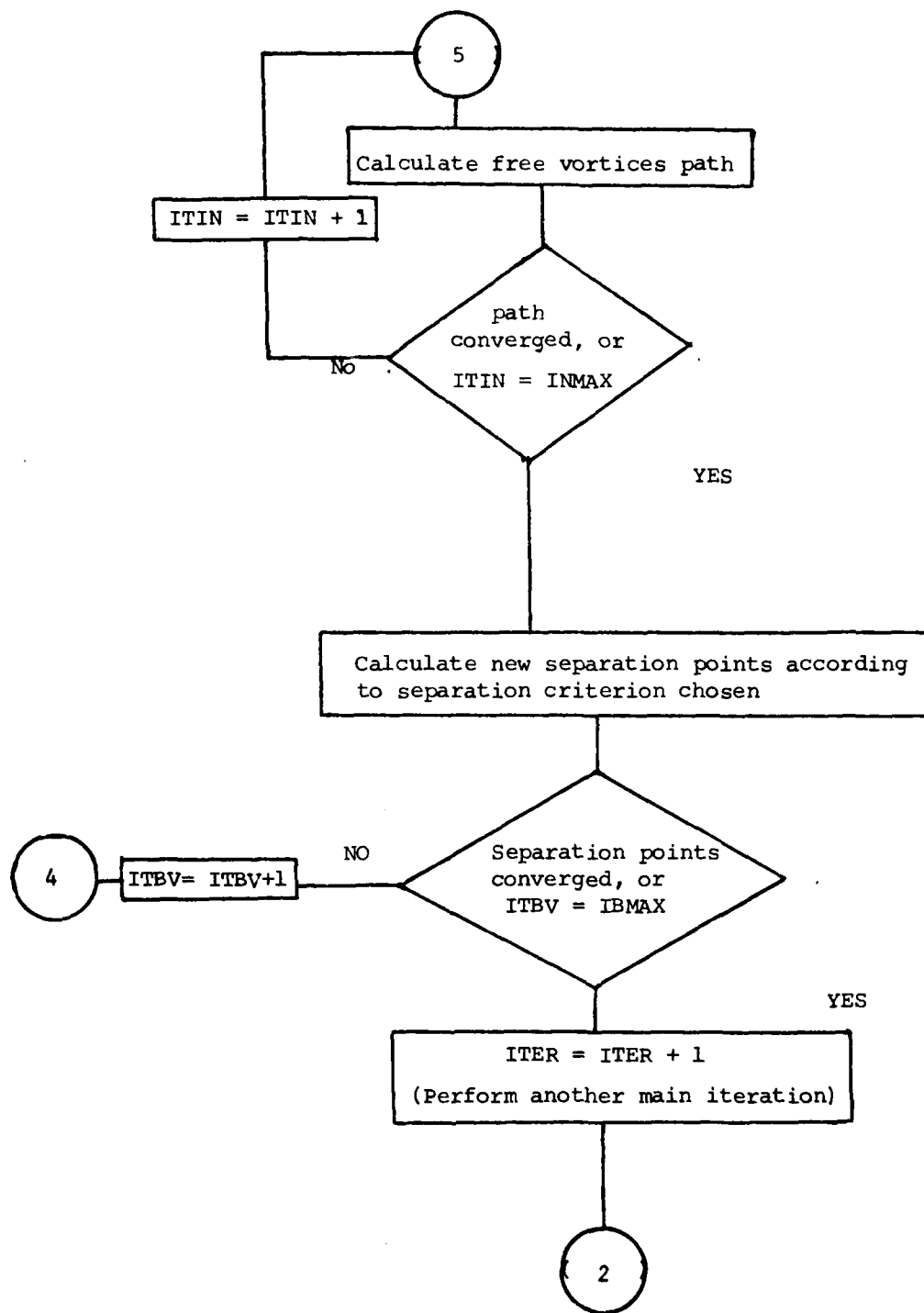


FIGURE No. 30 - CONTINUED.

